Chen *et al. Energy Mater* 2022;2:200028
DOI: 10.20517/energymater.2022.30

Energy Materials

Review

Open Access

Check for updates

Recent advances in earth-abundant first-row transition metal (Fe, Co and Ni)-based electrocatalysts for the oxygen evolution reaction

Xiaodong Chen[1,#], Jianqiao Liu[1,2,#], Tiefeng Yuan[2,#], Zhiyuan Zhang[2], Chunyu Song[3], Shuai Yang[4], Xin Gao[1,*], Nannan Wang[5,*], Lifeng Cui[1,*]

[1]College of Smart Energy, Shanghai Jiao Tong University, Shanghai 200240, China.
[2]School of Environmental Science and Engineering, University of Shanghai for Science and Technology, Shanghai 200093, China.
[3]Southern Marine Science and Engineering Guangdong Laboratory (Zhanjiang), Zhanjiang 524000, Guangdong, China.
[4]College of Chemistry and Chemical Engineering, Henan University of Technology, Zhengzhou 450001, Henan, China.
[5]College of Chemistry and Material Engineering, Chao Hu University, Hefei 238000, Anhui, China.
[#]These authors contributed equally to this work.

[*]**Correspondence to:** Dr. Xin Gao, College of Smart Energy, Shanghai Jiao Tong University, 665 Jianchuan Road, Minhang District, Shanghai 200240, China. E-mail: gx499708331@163.com; Prof. Nannan Wang, College of Chemistry and Material Engineering, Chao Hu University, 1 Bantang Road, Chaohu Economic Development Zone, Hefei 238000, Anhui, China. E-mail: nnw1990@126.com; Prof. Lifeng Cui, College of Smart Energy, Shanghai Jiao Tong University, 665 Jianchuan Road, Minhang District, Shanghai 200240, China. E-mail: cui@usst.edu.cn

How to cite this article: Chen X, Liu J, Yuan T, Zhang Z, Song C, Yang S, Gao X, Wang N, Cui L. Recent advances in earth-abundant first-row transition metal (Fe, Co and Ni)-based electrocatalysts for the oxygen evolution reaction. *Energy Mater* 2022;2:200028. https://dx.doi.org/10.20517/energymater.2022.30

Received: 19 May 2022 **First Decision:** 8 Jul 2022 **Revised:** 21 Jul 2022 **Accepted:** 28 Jul 2022 **Published:** 7 Aug 2022

Academic Editors: Yuping Wu, Yuhui Chen **Copy Editor:** Tiantian Shi **Production Editor:** Tiantian Shi

Abstract
The oxygen evolution reaction (OER) is of fundamental importance as a half reaction and rate-controlling step that plays a predominant function in improving the energy storage and conversion efficiency during the electrochemical water-splitting process. In this review, after briefly introducing the fundamental mechanism of the OER, we systematically summarize the recent research progress for nonprecious-metal-based OER electrocatalysts of representative first-row transition metal (Fe, Co and Ni)-based composite materials. We analyze the effects of the physicochemical properties, including morphologies, structures and compositions, on the integrated performance of these OER electrocatalysts, with the aim of determining the structure-function correlation of the electrocatalysts in the electrochemical reaction process. Furthermore, the prospective development directions of OER electrocatalysts are also illustrated and emphasized. Finally, this mini-review highlights how systematic introductions will accelerate the exploitation of high-efficiency OER electrocatalysts.

Keywords: OER, catalytic mechanism, catalytic performance, first-row transition metal-based electrocatalysts, structure-function correlations

INTRODUCTION

The unrestricted consumption of traditional fossil fuels not only aggravates the global energy crisis but also causes significant damage to the natural ecological environment[1-4]. Therefore, it is extremely urgent to push forward extensive research into renewable clean energy sources, such as solar energy, wind energy, H_2 energy, and so on[5-9], as alternatives for non-renewable fossil fuels. Among these, H_2 can be considered as the most promising renewable clean energy source due to its inherent advantages of all-weather utilization, extensive sources, zero-pollutant emission and high combustion value[10-12]. Realistically, the vigorous development of H_2 production technologies is a prerequisite for its commercial utilization[12,13]. In this regard, the H_2 production derived from electrochemical water-splitting can be served as a preferential selection, owing to its approvable characteristics of the earth abundance and accessibility of water recourses and particularly the clean, large-scale and sustainable hydrogen production, which makes it more feasible for commercialization[14].

The water electro-dissociation procedure consists of two essential half reactions, namely, the hydrogen evolution reaction (HER) and the oxygen evolution reaction (OER), which simultaneously occur on the cathode and anode of the water-splitting alkaline electrolyzer respectively[15]. The water-splitting process exhibits a thermodynamically endothermic reaction and requires a thermodynamics Gibbs free energy (ΔG) of 237.2 kJ mol^{-1}, corresponding to a standard potential (ΔE) of 1.23 V *vs.* a reversible hydrogen electrode (RHE)[16]. Nevertheless, compared with the two-electron transfer HER, the OER is the rate-determining step due to its sluggish kinetics as a consequence of the four-electron transfer in the formation of the O=O bond, which eventually controls the integrated energy transformation efficiency of the electrochemical water-splitting process[17,18]. Thus, the fabrication of high-efficiency OER electrocatalysts is essential for reducing the kinetic energy barriers, which is the key to realizing their industrial application.

To date, noble metal-based materials, including RuO_2 and IrO_2, are recognized as the benchmark OER electrocatalysts because they are well known for their high-performance OER activities. Unfortunately, their intrinsic disadvantages of high expenditure and low abundance have restricted their commercial large-scale application[19,20]. Thus, multiple efforts have been executed to develop earth-abundant first-row transition metal-based electrocatalysts, such as typical oxides[21], carbides[22,23], sulfides[24,25], selenides[26,27], nitrides[28] and phosphides[29,30], which have made the greatest contribution to OER activities[31]. Accordingly, it is essential to directly carry out investigations and summaries of these materials as efficient OER electrocatalysts[32].

In this review, we concentrate on the catalytic performance of earth-abundant first-row transition metal (Fe, Co and Ni)-based composite materials as electrocatalysts, which are demonstrated to be a subject of increasing interest. More specifically, the physicochemical properties of these electrocatalysts, such as the morphologies, compositions, promoting abilities and presence of metal-support interactions, which are mainly responsible for the OER electrocatalytic activities, are systematically introduced to elucidate their structure-activity relationships. Furthermore, the prospective exploitation direction of OER electrocatalysts is also illustrated and emphasized. This mini-review provides general guidelines for the state-of-the-art architecture of OER electrocatalysts and a discussion of their challenges and further prospects.

OER ELECTROCATALYTIC SYSTEMS

Noble metal-based materials were the first electrocatalysts used for hydrogen production by electrocatalytic water splitting[33]. As far as elemental noble metal electrocatalysts are concerned, the corresponding order of OER catalytic activity is as follows: Pt < Rh < Pd < Ir < Ru. Kim *et al.*[34] found that in the OER process, although the high operating potential causes the oxidation of Ru and Ir surfaces to produce RuO_2 and IrO_2, respectively, these oxides have the characteristics of high conductivity and excellent electronic structure, so they still maintained excellent OER catalytic activities. Hu *et al.*[35] summarized the OER catalytic properties of Ru, Ir and their corresponding oxides. It was demonstrated that the order of catalytic activities is Ru > Ir ≈ RuO_2 > IrO_2. Although RuO_2 and IrO_2 exhibited excellent catalytic activity under acidic and alkaline conditions, their corrosion resistance was undesirable and thus their stability needed to be further improved by compounding them with other metals or metal oxides. At present, the reported Ir-based composite electrocatalysts mainly included IrM (M = Cu, Fe, Co or Ni), IrCoNi, IrCuNi, IrO_2 and MO_x (M = Nb, Ti, Ta or Zr). These composite Ir-based electrocatalysts delivered excellent integrated OER performance[36]. For Ru-based composite electrocatalysts, the only $Ru_xIr_{1-x}O_2$ bimetallic oxide system formed by successful doping Ir into RuO_2 has been reported, which not only effectively inhibited the decomposition of the electrocatalyst but also significantly improved the OER catalytic stability[37].

In short, noble metal-based materials present excellent OER electrocatalytic activities but their commercial-scale applications are restricted by the inherent drawbacks of easy corrosion, scarcity and high cost[38]. Therefore, the key to the development of OER electrocatalysts is seeking transition metal materials with abundant reserves, low cost and high activity potential. In this regard, considering that transition metal materials are easily susceptible to oxidation and the corresponding high-valence metal ions have more oxidation properties during the OER electrochemical process, the representative earth-abundant first-row transition metal (Fe, Co and Ni)-based composites as OER electrocatalysts have attracted widespread attention and have been demonstrated to possess excellent performance for the OER.

Iron-based electrocatalysts

Fe has become the most attractive metal for OER electrocatalysts because of its high intrinsic conductivity, low toxicity and negligible and inexhaustible impact on the environment[39]. It has been concluded that although a single iron electrocatalyst can give poor OER activity, it can also serve as a promoter of polymetallic OER electrocatalysts[40,41]. For example, Dutta *et al.*[42] developed a Fe_3O_4/Ni_xP electrocatalyst with the architecture of an amorphous Ni_xP shell and a crystalline Fe_3O_4 core. It is noteworthy that the Fe_3O_4 nucleus in the electrocatalytic structure could activate the electrochemical process of Ni and therefore significantly improve the OER electrochemical activity. Zhang *et al.*[43] synthesized a NiFe layer double hydroxide-supported Au electrocatalyst (Au/NiFe-LDH), which delivered a low overpotential for the OER (η_{10} = 237 mV) and high durability. Density functional theory (DFT) calculations illustrated that Fe in the Au/NiFe-LDH should be the active center of the OER and Au could simultaneously help to control the charge distribution of the hybrid by transferring electrons to the LDH, so as to synergistically contribute to the overall performance of the OER catalytic activity. Sun *et al.*[44] found that when compared with the activities of $Co(OH)_2$ and Fe_3O_4 (η_{10} = 480 and 540 mV, respectively), $Co(OH)_2$ nanosheets (NSs) modified with Fe_3O_4 as OER electrocatalysts presented a higher OER activity (η_{10} = 390 mV). This was mainly attributed to the fact that the addition of Fe could optimize the electronic structure and surface properties of the electrocatalyst, which effectively promoted the transformation of intermediates during the OER catalytic process.

Feng *et al.*[45] synthesized FeOOH/Co/FeOOH-HNTA/NF hybrid electrocatalysts with anisotropic and hollow nanostructures. Due to the eminent synergistic effect between the FeOOH and Co layers in the material, not only was the conductivity of the Co metal central layer improved but a convenient channel for electron transmission during the OER process was also provided to improve the OER electrocatalytic activity. Zhang *et al*.[46] fabricated a gelation FeCoW hydroxyl oxide electrocatalyst. On account of the excellent synergistic effect of the Fe, Co and W elements in the structure, it provided favorable electronic structure and coordination environment for the effective water oxidation reaction, thus enhancing the catalytic performance of the OER. Zhang *et al*.[47] prepared polyaniline-coated Prussian blue analogs as multifunctional catalytic materials for total electrolytic water (PBAs@PANI). By accurately controlling the reaction parameters, PANI was evenly wrapped on the surfaces of the PBA nanocubes and the thickness of its shell could be easily adjusted. This advanced nanostructure could significantly enhance the charge transfer, elastic buffer and corrosion protection, thus accelerating its OER catalytic performance. Zhang *et al*.[48] took advantage of a pyrolysis method to bind the active sites of Ni(Fe)OOH and Ni/Fe-N-C to three-dimensional (3D)-interconnected PANI nanochains (Ni_2Fe_1@PANI-KOH900) [Figure 1]. In this regard, the PANI matrix not only improved the conductivity of the electrocatalyst but also maintained the stability of its chain structure, so as to obtain more electron channels for improving its bifunctional catalytic performance for the OER and ORR.

Dong *et al*.[49] confirmed that transition metal ion (TMI)-doped conductive polymers [such as Fe (III)-doped PANI] with foamed nickel could effectively accelerate the catalytic performance of the HER or OER. This was because the TM-N bond in the TMI-doped conductive polymers could produce active center sites with high activities, which significantly reduced the energy barrier of the HER or OER intermediates and relevant products. Liu *et al*.[50] synthesized amorphous cobalt iron hydroxide (CoFe-H) using a facile electrodeposition strategy as an efficient OER electrocatalyst to achieve photoelectrochemical water splitting. The CoFe-H/$BiVO_4$ photoanode was constructed with CoFe-H NSs and a $BiVO_4$ semiconductor, with a good photocurrent density was obtained. It was demonstrated that the improved OER kinetics and high-quality interface of CoFe-H/$BiVO_4$, as well as the excellent optical transparency of the CoFe-H NSs, contributed to the enhancement of the photoelectrocatalytic OER performance. Yang *et al*.[51] developed a ferroelectric-enhanced photoelectrocatalytic system using $BiVO_4$ and Co_3O_4 as photocatalysts and cocatalysts to couple $BiFeO_3$ to form $BiVO_4$-$BiFeO_3$ heterojunctions. The cocatalysts could provide the additional electrocatalytically active sites for OER and the $BiVO_4$-$BiFeO_3$ heterojunction promoted carrier separation and $BiFeO_3$ could form a local internal electric field through ferroelectric polarization at low voltage, which further promoted carrier separation and increased the photocurrent. Zhu *et al*.[52] used a facile electrodeposition synthesis method to fabricate NiFe-LDH-modified α-Fe_2O_3 photoanodes with enhanced photoelectrocatalytic OER performance. Compared with reversible hydrogen electrodes, the photocurrent density of α-Fe_2O_3/$Ni_{0.5}Fe_{0.5}$-LDH electrodes was much higher than that of bare α-Fe_2O_3 and it also exhibited good durability. Mott–Schottky and electrochemical impedance spectroscopy measurements indicated that the significant enhancement of the photoelectrocatalytic performance of α-Fe_2O_3/NiFe-LDH derived from the decrease in charge transfer resistance and the increase in carrier density.

Recently, Xu *et al*.[53] synthesized a nickel-iron diselenide ether derived oxide ($Ni_xFe_{1-x}Se_2$-DO) electrocatalyst and compared its OER electrocatalytic activity with a NiSe-DO electrocatalyst. The results illustrated that the OER overpotential of the $Ni_xFe_{1-x}Se_2$-DO electrocatalyst (η_{10} = 195 mV) was lower than that of the NiSe-DO electrocatalyst (η_{10} = 253 mV), so the addition of Fe substantially improved the OER electrocatalytic activity of the $Ni_xFe_{1-x}Se_2$-DO electrocatalyst. Hung *et al*.[54] carried out an in-depth study of the effect of the geometric position of Fe and Co ions in an iron-doped cobalt oxide electrocatalyst ($CoFe_y$) with different mass ratios on the OER activity. It was found that the OER activity increased with increasing Fe content in $CoFe_y$ ($CoFe_0 < CoFe_{0.16} < CoFe_{0.28} < CoFe_{0.38} < CoFe_{0.44}$). The XAS characterization demonstrated that the Fe ions occupied the octahedral position [Fe^{3+} (OH)] in $CoFe_{0.44}$, while Co ions were limited to tetrahedral sites

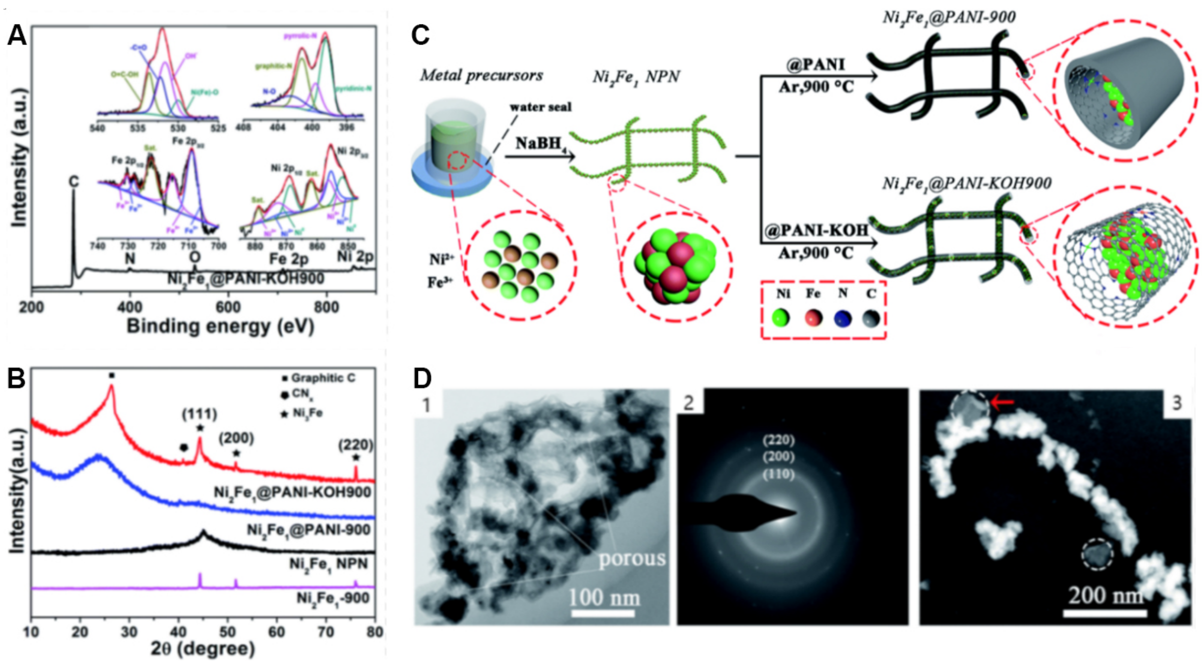

Figure 1. (A) XPS surface survey scan and high-resolution O 1s, N 1s, Fe 2p and Ni 2p spectra of Ni_2Fe_1@PANI-KOH900. (B) XRD patterns of Ni_2Fe_1-900, Ni_2Fe_1 NPN, Ni_2Fe_1@PANI-900 and Ni_2Fe_1@PANI-KOH900. (C) Schematic illustration of synthesis procedure for Ni_2Fe_1 NPN, Ni_2Fe_1@PANI-900 and Ni_2Fe_1@PANI-KOH900. (D) TEM (1), SAED (2) and HADDF-STEM (3) images of Ni2Fe1@PANI-KOH900. Reproduced with permission. Copyright 2019, Royal Society of Chemistry[48].

[Co^{2+} (Td)], which dramatically promoted the corresponding OER activities (η_{10} = 229 mV and η_{100} = 281 mV). Zhuang *et al.*[55] fabricated Fe_xCo_y-O NS electrocatalysts, which had the advantages of rich oxygen vacancies, high specific surface area and ultrathin thickness. Therefore, the NSs showed excellent OER performance in a 0.1 M KOH solution (η_{10} = 308 mV and ζ = 36.8 mV dec^{-1}). Jin *et al.*[56] investigated the effect of Fe and Mo doping on the OER activity of a $Ni(OH)_2$/NiOOH-NS electrocatalyst. As shown in Figure 2, when compared with the $Ni(OH)_2$/NiOOH-NSs (η_{100} = 400 mV), MoFe/$Ni(OH)_2$/NiOOH delivered an excellent OER activity (η_{10} = 280 mV) and high stability. This was mainly because the addition of Fe and Mo in the $Ni(OH)_2$/NiOOH-NSs could enable the occurrence of the synergistic effect of Fe and Mo, which strengthened the interaction ability between Ni and OER intermediate products, thus improving its electrocatalytic activity. Based on the above studies, it is well known that although Fe is not the active center, it plays a prominent role as the OER promoter in such electrocatalysts.

Furthermore, it has been confirmed that iron nitride or iron phosphide embedded in a 3D porous structure or grown on a conductive substrate can act as the OER active center. The porous structure and conductivity of such materials can facilitate the contact area of the electrolyte solution and the charge transfer capacity between the catalytic active sites and substrate[28]. For example, Yu *et al.*[57] utilized the thermal nitriding method to in-situ realize the fabrication of nanoporous membrane iron nitride (Fe_3N/Fe_4N) into a high-conductivity 3D graphene/nickel foam. This advanced architecture had the advantages of high specific surface area, abundant active sites, a porous structure and electrical conductivity, which were conducive to enhancing the mass transfer capacity of charge between the electrolyte and the electrode during the OER process, thus improving the corresponding electrocatalytic OER performance.

Realistically, the doping of Fe into electrocatalysts not only significantly accelerates the OER electrocatalytic activities but also plays an important role in improving the HER activities[58]. For example, Fan *et al.*[59]

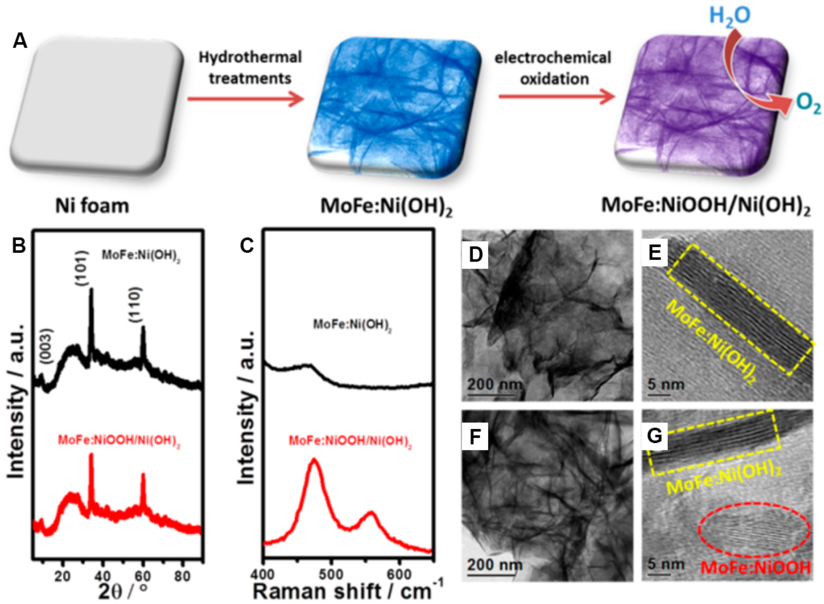

Figure 2. (A) Synthetic steps of forming MoFe:Ni(OH)$_2$/NiOOH NSs on nickel foam directly. (B) XRD patterns of MoFe:Ni-(OH)$_2$ and MoFe:Ni(OH)$_2$/NiOOH NSs. (C) Raman spectra of MoFe:Ni(OH)$_2$ and MoFe:Ni(OH)$_2$/NiOOH NSs. (D-G) TEM and HRTEM images of MoFe:Ni(OH)$_2$ and MoFe:Ni-(OH)$_2$/NiOOH NSs. Reproduced with permission. Copyright 2018, American Chemical Society[56].

doped Fe into Ni_3C-based NSs, indicating that suitable Fe doping could optimize the electronic properties and surface composition of Ni_3C and further improve the HER and OER catalytic performance. In particular, Ni_3C-based NSs (Fe-Ni_3C-2%) doped with 2 at.% Fe exhibited a low overpotential (292 mV) and small Tafel slope (41.3 mV dec^{-1}) for the HER in an alkaline solution, which presented the best performance. Liu *et al.*[60] prepared NiFe precursors using an electrodeposition strategy and then fabricated Ni_3FeN with not only a 3D porous structure but also interlinked nanoparticles in a NH_3 atmosphere at 400 °C. The results showed that Ni_3FeN has higher HER catalytic activity than Ni_3N and Fe_2N (Ni_3FeN: η = 105 mV at 10 mA·cm^{-2} in 1.0 M KOH). Deng *et al.*[61] successfully synthesized FeCo nanoparticles in N-doped carbon nanotubes, which offered an excellent performance of η_{10} = 110 mV with ζ = 74 mV dec^{-1}. Its electrocatalytic activity mainly originated from Fe and Co alloying and their encapsulation in the conducting carbon nanotubes reduced the charge transfer resistance during the HER process.

Furthermore, considerable studies also disclosed that iron selenide, phosphide and sulfide exhibited excellent HER electrocatalytic performance. For example, Theerthagiri *et al.*[62] immobilized iron diselenide ($FeSe_2$) nanorods on graphene oxide NSs, which showed a better performance of $\eta_{9.68}$ = 250 mV and ζ = 64 mV dec^{-1}. Zhang *et al.*[63] synthesized $Ni(OH)_2$-Fe_2P by electrodeposition using Fe_2P as a precursor, where the amorphous $Ni(OH)_2$ was deposited on crystalline Fe_2P and had a nanoarray structure. The electrocatalyst had good catalytic activity and stability, as well as excellent HER activity (η of 76 mV at 10 mA·cm^{-2}). Furthermore, Guo *et al.*[64] synthesized graded hollow microspheres of FeP as HER electrocatalysts, which showed reasonable stability of η_{10} = 144 mV, ζ = 58 mV dec^{-1} and 1000 CV cycles. Similarly, Zhu *et al.*[65] reported hollow mesoporous FeP-coated with a carbon layer (HMFeP@C). The results illustrated that the electrocatalysts exhibited a lower η_{10} value (115 mV), higher stability (constant j for 20 h) and similar ζ (56 mV dec^{-1}). Due to the synergistic interaction between the cubic and porous structures, it displayed good HER catalytic activity and stability.

Recently, Chung *et al.*[66] synthesized FeP NPs coated with carbon shells (FeP/C), exhibiting the high electrocatalytic activity and stability of η_{10} = 71 mV, ζ = 52 mV dec^{-1} and 5000 CV cycles, with no significant change in performance [Figure 3]. The high stability was attributed to the coated carbon shell, which effectively protected the FeP NPs from oxidation under the HER. Konkena *et al.*[67] reported the study of nickel-chromite-iron ore with a composite of $Fe_{4.5}Ni_{4.5}S_8$ as a HER electrocatalyst, which delivered excellent activity and stability in a 0.5 M H_2SO_4 solution (η_{10} = 280 mV and ζ = 72 mV dec^{-1}). Yu *et al.*[68] synthesized hierarchical porous microflowers of 3D-ferric nickel sulfide on foamed nickel ($Ni_{0.7}Fe_{0.3}S_2$/NF) by a hydrothermal sulfidation method. Due to the synergistic effect of the Fe-Ni alloy and the doping of S, the charge resistance in the reaction process was reduced, so the electrocatalyst had good HER electrocatalytic activity in a 1 M KOH solution (η_{10} = 155 mV). In addition, Li *et al.*[69] prepared ultrathin $CuFeS_2$ NSs, delivering better electrocatalytic performance of η 10 = 88.7 mV, ζ = 47 mV dec^{-1}, JE = 0.35 mA·cm^{-2} and 15 000 CV cycles in a 0.5 M H_2SO_4 solution. DFT calculations showed that the HER activity of $CuFeS_2$ NSs was attributed to the high-density exposure of active S^{2-} species.

Cobalt-based electrocatalysts

Cobalt oxide

It has been demonstrated that among non-noble metal oxides, the representative Co_3O_4 has the lowest theoretical overpotential for the OER. Therefore, efficient Co_3O_4-based electrocatalysts for the OER could be designed by changing their morphology and structural composition[70]. There are two different oxidation and coordination environments for Co atoms in Co_3O_4, namely, tetrahedral coordination Co (II) (Co^{2+} Td) with an intermetallic distance of 3.36 Å and octahedral coordination Co (III) (Co^{3+} Oh) with intermetallic distances of 2.85 and 3.36 Å. In the anodic potential region before the initial potential, the cobalt oxyhydroxide (β-CoOOH) intermediates transformed from Co^{2+} Td possess a stronger water oxidation ability than pure Co_3O_4. Therefore, the catalytic activity of Co^{2+} Td could be further ameliorated by adjusting and increasing the ratio of Co^{2+} Td to Co^{3+} Oh [71]. Wang *et al.*[72] successfully synthesized a spinel $ZnCo_2O_4$ electrocatalyst containing only a Co^{3+} Oh center and a spinel $CoAl_2O_4$ electrocatalyst containing only a Co^{2+} Td center. EXAFS fitting illustrated that the conversion of Co^{2+} Td ion over the $CoAl_2O_4$ surface could generate a highly active β-CoOOH intermediate species during the OER process, which prominently reduced the energy barrier of the OER intermediates process, while the Co^{3+} Oh ions on the surface of $ZnCo_2O_4$ were oxidized to Co^{4+}, which barely exhibited catalytic activity for the OER.

Menezes *et al.*[73] prepared spinel Co_3O_4 nanoparticles partially substituted with Mn^{3+} (MCO) and introduced metal defect sites to the surface of MCO by removing Mn^{3+} ions in post-treatment [Figure 4]. The removal of Mn^{3+} ions from the octahedral position made the MCO surface with highly exposed Co^{2+} Td centers, which promoted the formation of active intermediates over the β-CoOOH during the OER process. Compared with the original electrocatalyst, the OER electrocatalyst that was rich in defect sites derived from MCO has a lower overpotential (η_{10} = 320 mV). Although the removal of the Co^{3+} Oh site makes the OER more feasible, it may have a negative impact on the electronic structure of the electrocatalyst and may significantly reduce its conductivity. Therefore, while maintaining the total amount of metal ions in the lattice, it was more practical to transform the octahedral Co^{3+} Oh center sites with lower activity into tetrahedral Co^{2+} Td center sites with higher activity. For example, Xu *et al.*[74] etched Co_3O_4 with oxygen plasma to remove the oxygen atoms on its surface and convert the high-valence Co^{3+} ions into low-valence Co^{2+} ions, so as to improve the abundance of Co^{2+} Td active center sites in Co_3O_4 and promote the efficient oxidative decomposition of water. In order to further improve the conductivity and activity of Co_3O_4, the anoxic Co_3O_4 could be hybridized with a high-conductivity carbon matrix, which provided a convenient channel for electron transfer during the OER process.

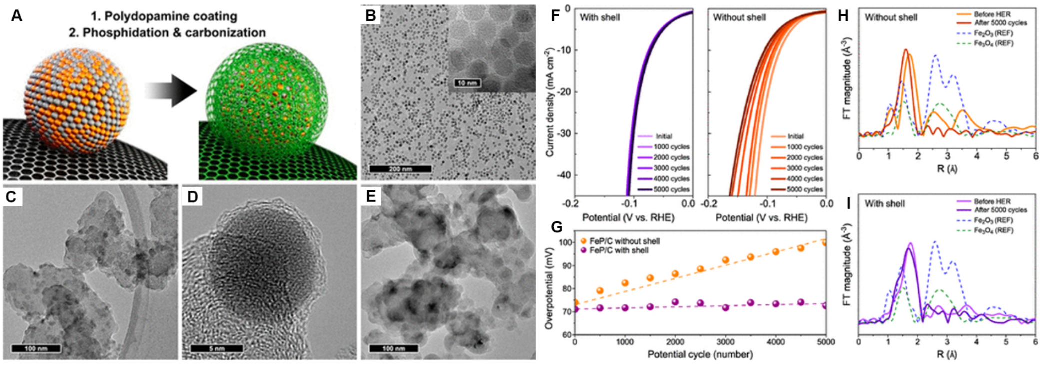

Figure 3. (A) Schematic representation of carbon shell-coated FeP NP preparation. TEM images of as-synthesized (B) iron oxide NPs, (C, D) carbon shell-coated FeP NPs and (E) FeP NPs prepared without a carbon shell. Long-term durability test of FeP/C electrocatalysts: (F) polarization curves for 5000 cycle tests of FeP NPs with (left) and without (right) a carbon shell. (G) Plots of overpotential *vs.* potential cycle. EXAFS analysis of FeP NPs (H) without and (I) with a carbon shell. Reproduced with permission. Copyright 2017, American Chemical Society[66].

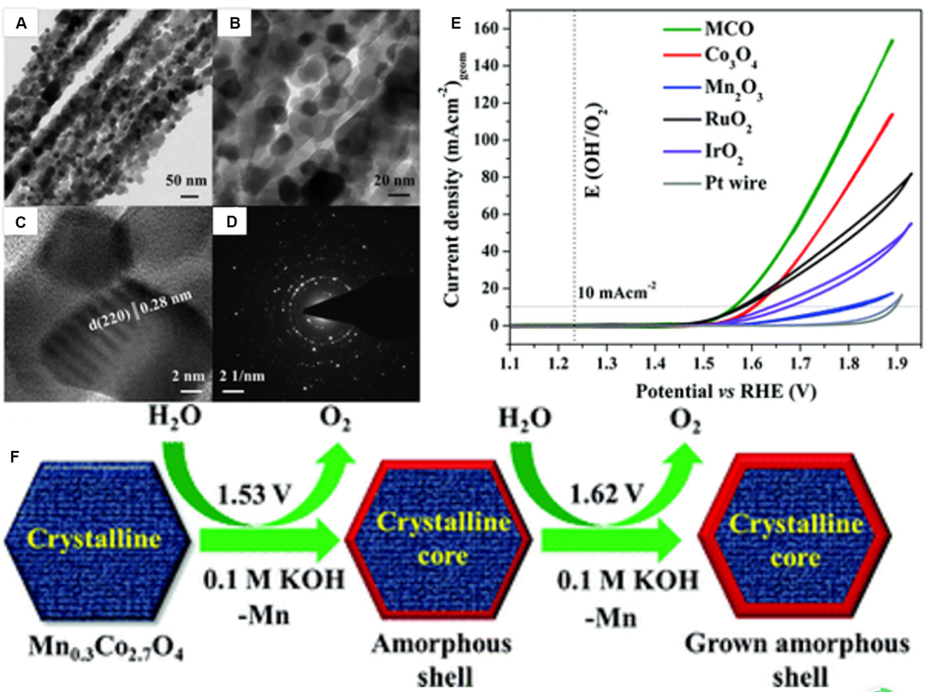

Figure 4. (A, B) TEM and (C) HRTEM images with d-spacing of 0.28 nm, indicating (220) plane, and (D) SAED pattern of MCO nanochains. (E) Cyclic voltammetry (CV) of MCO, Co_3O_4 and Mn_2O_3 synthesized by similar approach versus Mn_2O_3 and commercial noble electrocatalysts in a 1 M KOH solution with a scan rate of 20 mV s^{-1} on FTO substrates (loading of ~1 mg). (F) Near-surface structural reorganization of MCO at the onset and the elevated oxygen evolution potential. Reproduced with permission. Copyright 2017, Royal Society of Chemistry[73].

Tong *et al.*[75] synthesized ultrathin NSs (CoO_x NPs/BNG) of graphene that were rich in boron and nitrogen and coupled with anoxic CoO_x NPs. The reason for the enhanced activity of the OER electrocatalyst was intimately related to the oxygen defect structure of CoO_x, which not only regulated the electronic structure of the electrocatalyst, but also encouraged its own oxygen affinity. Furthermore, the formation of Co-N-C and Co-B-N bonds also increased the conductivity of the electrocatalyst and promoted the OER electron transfer of the Co metal center. Although adjusting the composition of Co^{3+} and Co^{2+} in Co_3O_4 provides a simple and feasible method to obtain a high-activity electrocatalyst, its poor conductivity still needs to be resolved. Therefore, the first row of transition metals, including Fe, Ni, Cu, Cr and V, could be doped into Co_3O_4 to alter its electronic band structure and increase its affinity for OER active species (O*, HO* and HOO*)[76]. For instance, Lin *et al.*[77] confirmed that embedding electrophilic Cr^{3+} ions ($Cr_{0.75}Co_{2.25}O_4$) in spinel cobalt oxide enhances the oxygen affinity of the central Co^{2+} sites. In addition, Cr^{3+} ions replaced Co^{3+} ions inert to the OER at the octahedral center [Figure 5A], which also enhanced the electron transport capacity of the whole electrocatalyst surface. Tahir *et al.*[78] loaded NiO/Co_3O_4 hybrid nanoparticles on N-doped carbon nanotubes as OER electrocatalysts. The XPS analysis showed that compared with NiO and Co_3O_4 NPs loaded alone, the Ni and Co atoms in the hybrid material had a high oxidation state and there was a strong coupling ability between the metal center and the N atoms in the carbon matrix. This enhanced the oxygen affinity and electronic conductivity and improved the OER electrochemical performance [Figure 5B]. Patel *et al.*[79] synthesized a semitransparent and porous p-type Co_3O_4 film and proved that it could be used for photoelectrocatalytic hydrogen production. Simultaneously, they found that the study of Co_3O_4 splitting seawater not only exhibited desirable photoelectrocatalytic HER activity but also contributed to the efficient formation of sea salt.

PANI has recently become the preferred choice for the preparation of electrocatalytic materials because of its simple monomer, convenient synthesis, strong plasticity, high conductivity and mechanical strength and stable chemical properties[80,81]. For example, Sun *et al.*[82] synthesized PANI@Co-Fe LDH-layered nanomaterials by a hydrothermal method, benefiting from the excellent conductivity of PANI and the two-dimensional layered nanosheet structure of Co-Fe LDHs, it delivered superior OER electrocatalytic activity (η_{10} = 261 mV and ζ = 67.85 mV dec^{-1}). Dang *et al.*[83] fabricated CoNiNDC/PANI-NF composites by reacting cobalt acetate and nickel acetate with 2,6-naphthalenediformate dipotassium and in-situ deposition of their products on a PANI-NF substrate. The PANI-NF could narrow the size of the CoNiNDC NSs and distribute them evenly on the surface, so that more active sites could be exposed to the outer surface, which would further contribute to the OER electrocatalytic activity.

In our research, we developed a facile and feasible strategy to realize the in-situ assembly of CoOOH NSs into a PANI network (Co/PANI NSs) for OER performance. The nitrogen species derived from PANI building blocks could function as bridging sites to preferentially coordinate with Co metal ions, which imparted coupling effects between CoOOH NSs and PANI, as well as structural stability. In addition to the Co-N coordination, the occurred electron delocalization between Co d-orbitals and PANI π-conjugated ligands could also modulate the electronic structural states of the Co/PANI HNSs, enabling the efficient interfacial electron transfer from CoOOH to PANI. Furthermore, the Co/PANI HNSs possessed a hierarchical porous with both mesopores and macropores that allowed electrolytes to be more efficiently transported to the highly oxidative active sites, resulting in fast reaction kinetics for the OER[84]. PANI had large amounts of amino and imino functional groups, which could provide lone-pair electrons and were easy to coordinate with transition metals, such as Co, so that the interaction between post-consumed PANI and hydroxides and metal oxides derived from these metals was enhanced, giving its composite surface excellent electronic structure and high structural stability[85,86].

In our group, novel defect-induced nitrogen-doped carbon-supported Co_3O_4 NPs were also successfully fabricated as OER electrocatalysts (denoted as Co_3O_4/CN HNPs) through a wetness-impregnation treatment of Co/PANI, followed by thermal annealing. This favorable architecture of the Co_3O_4/CN HNPs could not only improve their conductivity and electrocatalytically active sites but also generate a large number of oxygen vacancies and crystal defects. This effectively exerted the preponderance in facilitating the interfacial electronic transfer and optimizing the adsorption energy for intermediates, thus imparting the

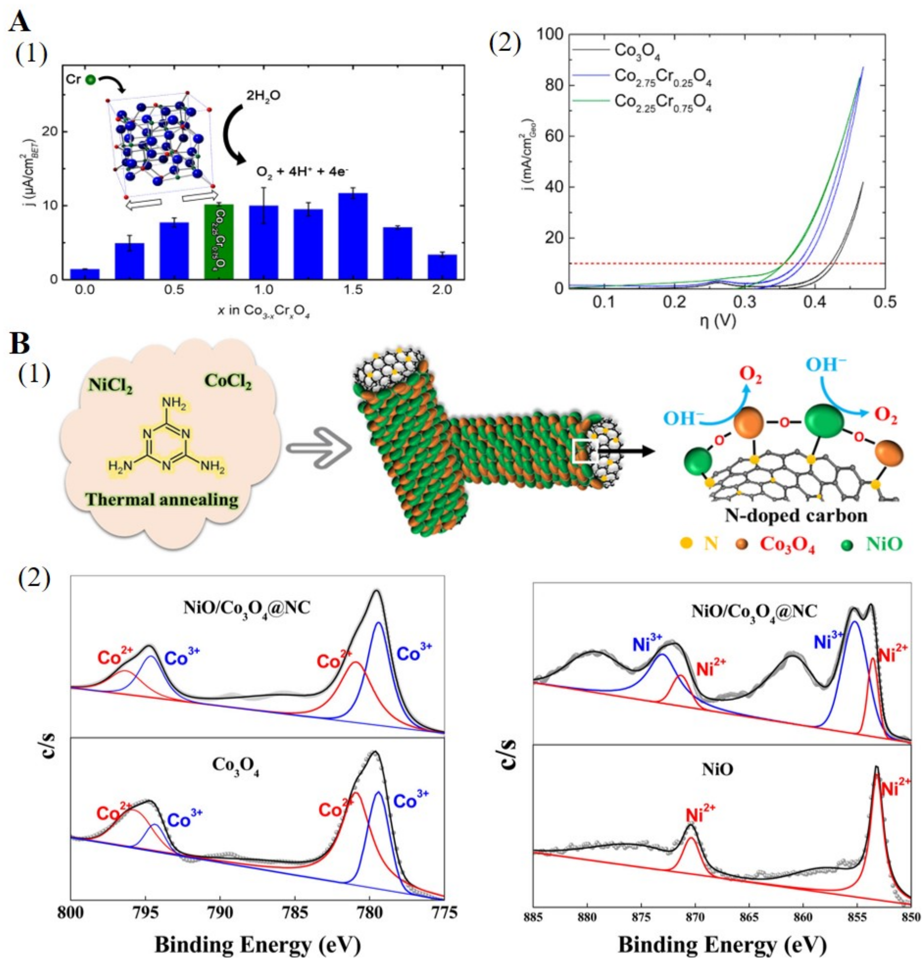

Figure 5. (A) Molecular structure of $Co_{3-x}Cr_xO_4$ electrocatalysts and energy density comparison by changing the (1) Cr content and (2) representative RDEVs of Co_3O_4 (black), $Co_{2.75}Cr_{0.25}O_4$ (blue) and $Co_{2.25}Cr_{0.75}O_4$ (green) in O_2-sparged 1 M NaOH. Reproduced with permission. Copyright 2017, American Chemical Society[77]. (B) (1) Synthesis process and schematic structure of NiO/Co_3O_4@NC and (2) XPS spectra of Co 2p and Ni 2p. Reproduced with permission. Copyright 2017, American Chemical Society[78].

extraordinary activities in catalyzing the OER. In addition, there was evidence demonstrating the formation of C-N coordination bonds through the strong interaction of the interconnected interface and the generation of pyridinic-N species after the annealing treatment. These factors enabled the structural stability to obtain further strength and accelerated the oxygen release for the reduction of the OER overpotential, respectively[87].

Cobalt phosphide

Although Co_3O_4 has the highest stability and corrosion resistance in the OER process, its intrinsic catalytic performance is significantly lower than that of cobalt phosphide (CoP_x). This is because the electronegativity difference between the Co and P atoms in cobalt phosphide (Co_2P, CoP and CoP_2) is very small, so it exhibits high inherent conductivity, resulting in stronger metal properties[88]. In addition, under the condition of anodic polarization, the surface of CoP_x is oxidized to produce a CoO_x active layer. These CoO_x layers are mainly composed of cobalt (oxygen) hydroxyl species, similar to the β-CoOOH active intermediate in Co_3O_4, which is the main reason why water is easy to oxidize[89]. For example, Chang *et al.*[90] prepared a carbon-supported CoP nanorod electrocatalyst (CoP-NR/C). After anodic polarization, the surface of the CoP electrocatalyst was oxidized to nanosized CoO_x, thus improving the OER electrocatalytic activity. Moreover, the catalytic performance of CoP_x could be further enhanced by doping it with transition metals. The introduction of transition metals into the lattice could change the electronic structure of CoP_x, so as to adjust the binding energy of OER intermediate species at the Co center site, which considerably reduced the free energy of HOO* and O* intermediate species in the OER rate-controlling step. Xiao *et al*.[91] identified that metal-doped CoP_x electrocatalysts could produce excellent OER performance. Preeminent OER electrocatalysts could be obtained by doping with transition metal cobalt phosphide NSs (CoM-P-NS, M = Cu, Zn or Mn) [Figure 6]. DFT calculations demonstrated that the incorporation of Ni into the CoP lattice could decrease the ΔGo* of the OER in the rate-controlling step from 1.62 to 1.57 eV, sequentially promoting the release of O_2. Similarly, Mendoza-Garcia *et al*.[92] prepared $(Co_{0.54}Fe_{0.46})_2P$ nanoparticles doped with Fe and Co as electrocatalysts, revealing preferable OER electrocatalytic performance. Generally, the metal properties of CoP_x make it a promising OER electrocatalyst and its activity can be adjusted by heteroatom doping strategies.

Cobalt sulfide

For OER cobalt-based electrocatalysts, although the water oxidation performance of cobalt sulfide is inferior to cobalt oxide or cobalt phosphide, it still remains the focus of cobalt-based electrocatalytic materials. At present, cobalt sulfide, such as Co_3S_4, $Co_{1-x}S$, CoS_2, CoS and Co_9S_8, has been frequently utilized as OER electrocatalysts but their catalytic performance is severely restricted by low conductivity and reduced exposure of active sites. Therefore, increasing their specific surface area and complex synthesis with high conductivity heteroatom doped carbon matrix is the most effective strategy to address the above-mentioned challenges[72,73]. For example, Ganesan *et al*.[93] *in situ* grew cobalt sulfides of CoS_2 and Co_9S_8 phases on N, S-Co-doped graphite oxide plates, showing good OER electrocatalytic performance. Similarly, Qiao *et al*. [94] confirmed that $Co_{1-x}S$ hollow nanospheres ($Co_{1-x}S$/N, S-G) hybridized with graphene NSs doping with N and S heteroatoms had excellent electrocatalytic activity as OER electrocatalysts. This was mainly due to the hollow structure of cobalt sulfide nanoparticles in the electrocatalyst, with most of their active centers being completely exposed. Otherwise, O was directly doped in CoS_x lattice, resulting in the formation of a Co active center ΔGo*, which obviously contributes to the further release of O_2.

Cai *et al*.[95] synthesized an oxygen-doped cobalt sulfide porous nanocube ($CoS_{4.6}O_{0.6}$) electrocatalyst [Figure 7] and its OER catalytic activity was equivalent to the RuO_2 benchmark electrocatalyst. In addition to non-metallic doping, transition metal doping can also improve the OER properties of cobalt sulfide. For example, Cu doping could provide more O-binding sites for a Co_3S_4 electrocatalyst and optimize its electronic structure, hence improving the catalytic performance of the OER. Chauhan *et al*.[96] prepared layered nanosheet aggregates of $CuCo_2S_4$ as OER electrocatalysts, which exhibited a high specific surface area and interconnected nanosheet structure, thus ensuring the high conductivity and availability of active sites for excellent OER electrocatalytic performance. Sun *et al*.[97] first obtained self-supporting layered electrode materials by plating a PANI network layer on foam nickel and determined the growth position and orientation of $CuCo_2S_4$ nanoarrays. The nitrogen species from PANI could be combined with metal ions as the bridge sites, which provided a strong coupling effect for the in-situ growth of $CuCo_2S_4$ nanoarrays. Furthermore, the grid structure of PANI could divide the growth region into many smaller nanoblocks. Compared with the nitrogen sites evenly distributed on the mesh plane, only a small part of the nitrogen sites were located on the narrow fence structure, which made it difficult for $CuCo_2S_4$ to grow to the fence area, thus limiting its self-growth space. These nitrogen sites evenly distributed on the reticular plane could make $CuCo_2S_4$ grow perpendicular to its surface and limited their growth size simultaneously and this excellent structural feature could further enhance its OER electrocatalytic activity.

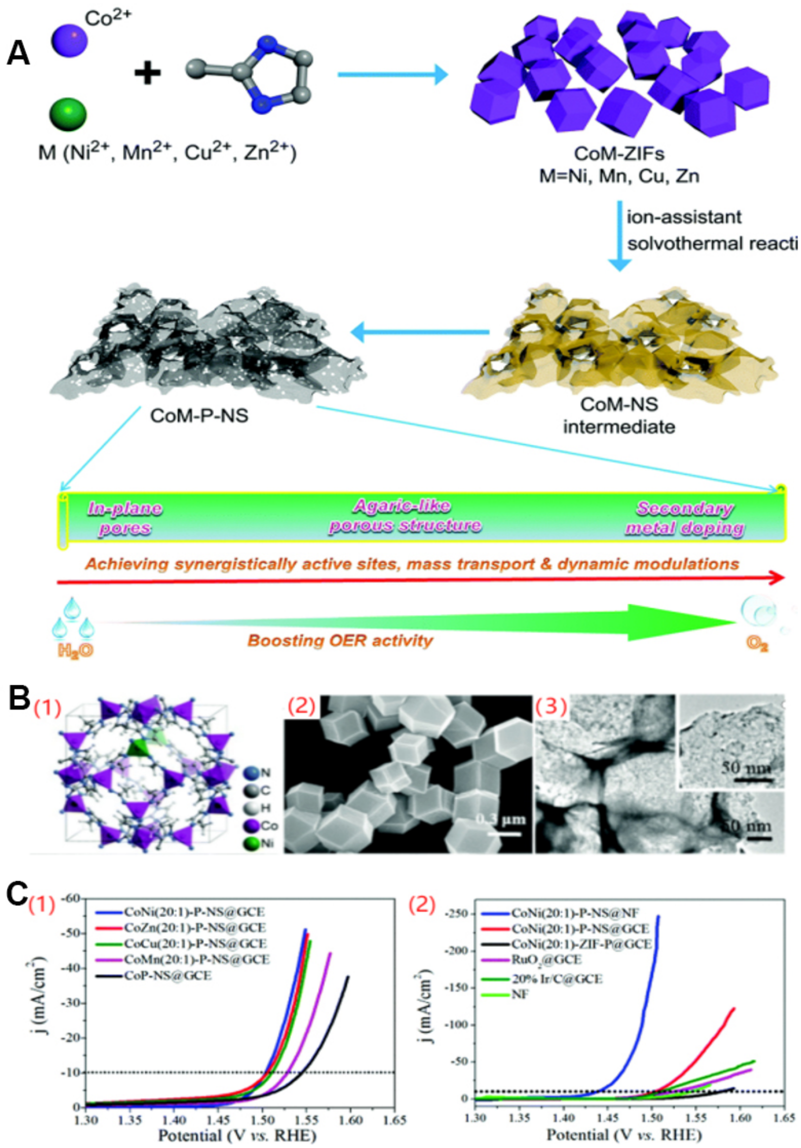

Figure 6. (A) Schematic illustration of a general synthetic approach to CoM-P NSs for high-efficiency OER derived from bimetallic MOFNs. (B) (1) Crystal structure, (2) SEM image of CoNi(20:1)-ZIF precursor and (3) TEM. (C) (1) Polarization curves of CoP-NS and CoM(20:(1)-P-NS (M = Ni, Mn, Cu or Zn) and of (2) CoNi(20:1)-P-NS on GCE or Ni foam (NF), CoNi(20:1)-ZIF-P. Reproduced with permission. Copyright 2017, Royal Society of Chemistry[91].

Shit *et al.*[98] developed a noble metal-free cobalt sulfide nanoparticle-grafted porous organic polymer nanohybrid (CoS_x@POP) as a photoelectrocatalyst. Its good photoelectrocatalytic activity for the HER could be attributed to the intrinsic synergistic effect of CoS_x and POP, which formed a unique high-porosity CoS_x @POP nanostructure. This structure permitted the easy diffusion of electrolytes and efficient electron transfer from POP to CoS_x during hydrogen generation with a tunable bandgap, which straddled between the reduction and oxidation potential of H_2O. Zhou *et al.*[99] prepared a CoS/$BiVO_4$ photoanode through surface modification by electrochemically modifying CoS onto the $BiVO_4$ surface. The resulting CoS/$BiVO_4$ photoanode exhibited a significantly enhanced photocurrent of 3.2 mA·cm^{-2} compared to a RHE under 1.23 V illumination, which was ~2.5 times higher than that of pristine $BiVO_4$. This surficial modification strategy was proven to be a favorable method to effectively enhance the photoelectrocatalytic OER activity.

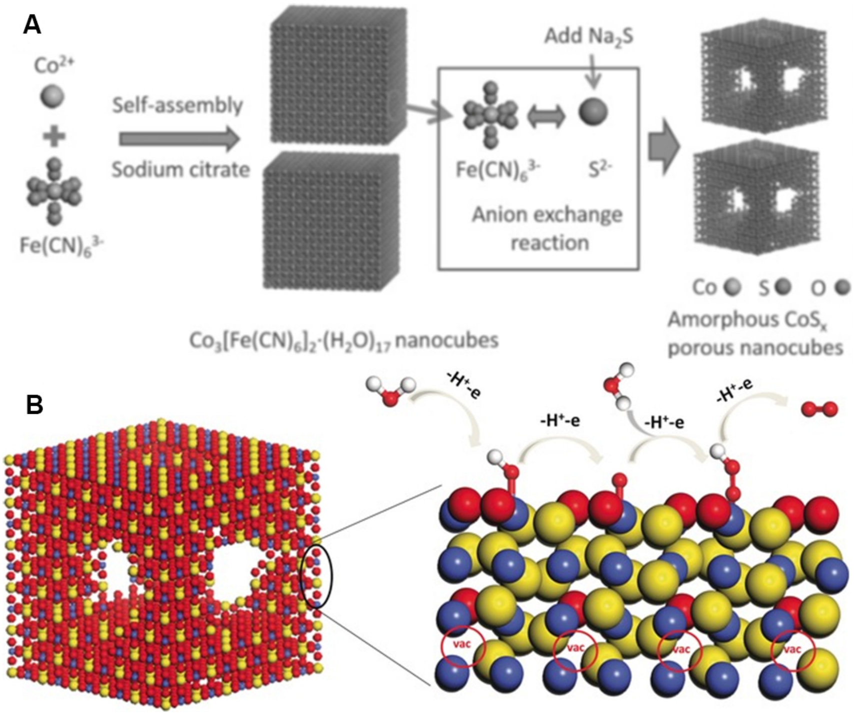

Figure 7. (A) Schematic of the synthesis process of A-$CoS_{4.6}O_{0.6}$ PNCs. (B) Schematic of oxygen-containing amorphous cobalt sulfide porous nanocubes with Co-S dangling bands, a distorted $CoS_{4.6}O_{0.6}$ octahedral structure and incorporated oxygen in the CoS_x (vac = vacancy, Co = blue, S = yellow, O = red and H = white). Reproduced with permission. Copyright 2017, Wiley[95].

Nickel-based electrocatalysts

Nickel and nickel alloys

Due to Ni being a 3D transition metal with earth-abundant sources, Ni-based electrocatalysts have the advantages of low expenditure, excellent electrocatalytic activity, outstanding stability and a high alloying degree with other metals. Ni electrocatalysts have important applications in the catalytic reaction of many industrial processes, especially in the fields of hydrogenation, secondary alkaline battery and water electrolysis[100]. It has been demonstrated that although Ni electrocatalysts exhibit superior OER electrocatalytic activity, they are vulnerable to corrosion, thus leading to final degradation in the consecutive reaction process[101]. As a consequence, the OER electrocatalytic performance of Ni electrocatalysts could be further enhanced by covering a conductive carbon layer on the electrocatalyst or providing support to prevent its agglomeration. For example, Ramakrishnan *et al*.[102] encapsulated Ni nanoparticles derived from Ni organic complexes in nitrogen-doped mesoporous carbon nanostructures (NCNPs) [Figure 8A], which displayed remarkable OER electrocatalytic performance in alkaline solutions. Li *et al*.[103] assembled FeNi bimetallic nanoparticles on a MOF-derived carbon matrix as an OER electrocatalyst (FexNiy-BDC, BDC = benzenedicarboxylate) [Figure 8B]. In this regard, the porous structure of the MOF-derived carbon matrix provided a broad specific surface area and the electronic synergy between Fe and Ni stabilized the OER active components of this electrocatalyst. Therefore, the FexNiy-BDC electrocatalyst presented better OER electrocatalytic performance. Wang *et al*.[104] utilized a MOF-74 derived matrix to anchor NiCo/Fe_3O_4 hybrid nanoparticles and used them as OER electrocatalysts [Figure 8C]. DFT calculation showed that NiCo species could promote the stability of the OER active species in the electrocatalytic process. In addition, the synergistic effect between Fe_3O_4 and NiCo in the NiCo/Fe_3O_4 hybrid materials also helps to boost the OER electrochemical activity.

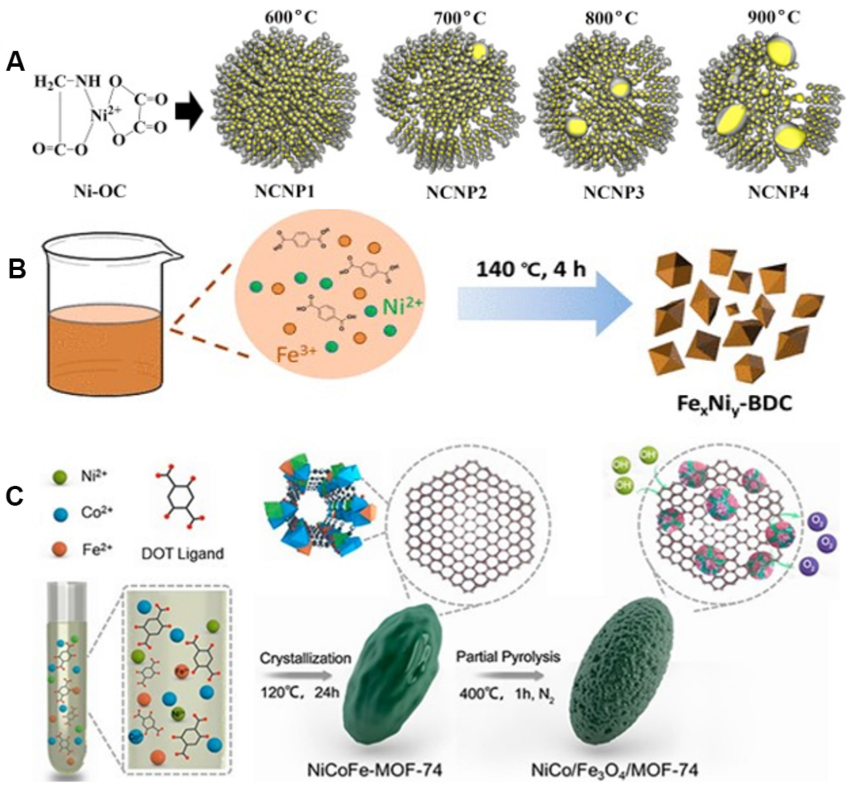

Figure 8. (A) Schematic representation of NCNP composite synthesis. (B) Schematic of FexNiy-BDC synthesis. (C) Schematic of NiCo/Fe_3O_4/MOF-74 synthesis. Reproduced with permission. Copyright 2019, Elsevier[102].

Nickel selenide

Matching metal Ni, nickel selenide ($NiSe_2$) has been examined for a wider range of applications and can easily be synthesized or grown with various porous nanostructures with high conductivity and specific surface area. $NiSe_2$ can be converted into nickel oxide and hydroxide at oxidation potentials as an active species of OER electrocatalysts. In addition, $NiSe_2$ deposited on a conductive carbon matrix or alloyed with other transition metals could significantly improve its OER electrocatalytic activity and stability[105]. Swesi *et al.*[106] fabricated metal-rich $NiSe_2$ on a gold-plated silicon substrate using an electrodeposition strategy. The electrodeposited $NiSe_2$ film containing Ni-Ni bonds had a phase structure similar to that of the sulfur mineral heap iron ore. Due to annealing at 300 °C, more Se defect sites were introduced, so the catalytic efficiency and overall crystallinity of the electrocatalyst were accordingly improved. Gu *et al.*[107] prepared iron-doped nickel selenide electrocatalysts (Fe-$NiSe_2$-UNWs) and investigated their effect on the OER performance [Figure 9]. The results demonstrated that in a 0.1 M KOH solution, the 8.4% Fe/$NiSe_2$ electrocatalyst had the best OER electrocatalytic performance (η_{10} = 268 mV and ζ = 41 mV dec^{-1}). According to DFT calculations, Fe doping could adjust the electronic structure of $NiSe_2$, effectively reduce the energy barrier of OER intermediate species and improve the corresponding catalytic performance.

Liu *et al.*[108] developed a nickel selenide electrode with PANI surface functionalization (NiSe-PANI) [Figure 10]. The modified PANI layer finely modulated the surface electronic structure of NiSe, optimized the surface Se-rich structure of NiSe and improved the formation of Ni^{3+} active species. When NiSe-PANI was used as a bifunctional electrocatalyst for total electrolytic water reaction, the NiSe-PANI electrode exhibited significant electrocatalytic activity (η_{10} = 300 mV), equivalent to the performance of Pt and IrO_2 combined electrodes. Similarly, other PANI-functionalized nickel sulfur electrodes also exhibited good total

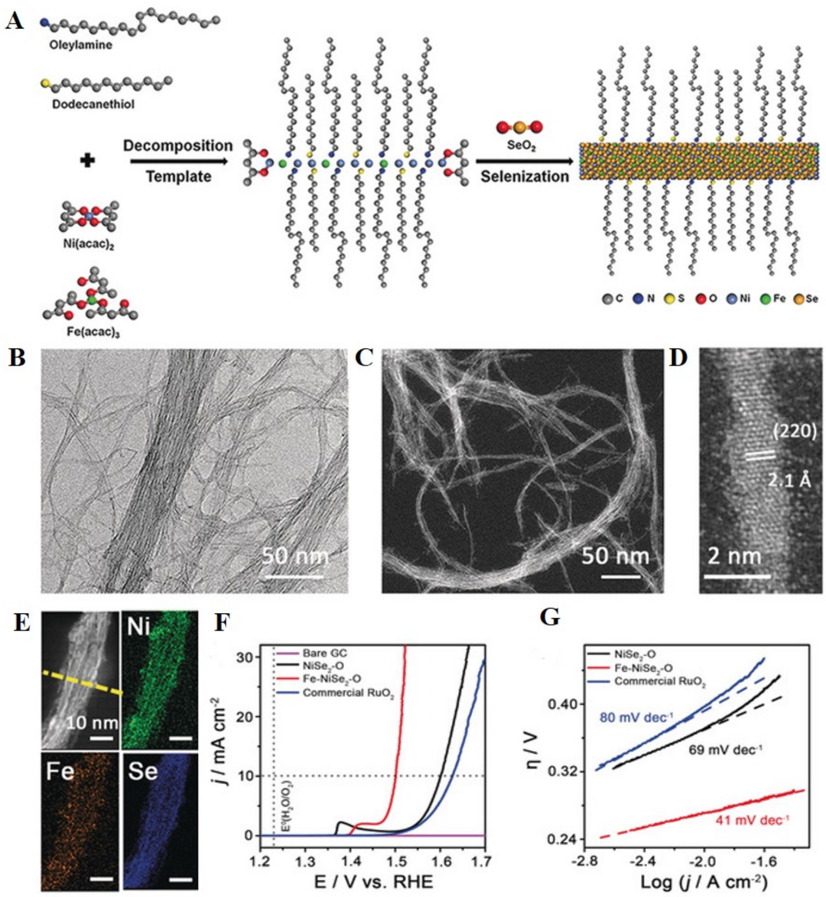

Figure 9. (A) Schematic illustration of the binary soft-template-mediated synthesis of Fe-$NiSe_2$ UNWs. (B) TEM image, (C) HAADF-STEM image, and (D) HR-HAADF image of Fe-$NiSe_2$ UNWs. (E) STEM-EDS elemental mapping images of Fe-$NiSe_2$ UNWs, showing the distribution of Ni green, Fe yellow, and Se blue. (F) Polarization curves for OER on bare GC electrode and modified GC electrodes composed of the pure and Fe-doped $NiSe_2$ samples and commercial RuO_2. Catalyst loading: 0.2 mg cm^{-2}. Sweep rate: 5 mV s^{-1}. (G) Tafel plots for corresponding catalysts derived from (F). Reproduced with permission. Copyright 2018, Wiley[107].

electrolytic water reaction performance, which proved that the electronic modulation strategy of PANI surface functionalization had universal applicability for improving the intrinsic OER electrochemical activity. Hou *et al.*[109] reported a 3D hybrid electrocatalyst that was constructed through the *in situ* anchoring of Co_9S_8 NSs onto the surface of Ni_3Se_2 NSs vertically aligned on an electrochemically exfoliated graphene foil. Benefiting from the synergistic effect between Ni_3Se_2 and Co_9S_8, it could be easily integrated with a macroporous silicon photocathode for highly active solar-driven photoelectrocatalytic water-splitting for the OER. Lee *et al.*[110] developed three possible polymorphic forms of nickel selenide (orthorhombic $NiSe_2$, cubic NiSe and hexagonal NiSe) as bifunctional electrocatalysts for photoelectrocatalytic systems. Photocathodes or photoanodes were fabricated by depositing the nickel selenide NCs onto p- or n-type Si nanowire arrays. Experiments revealed that compared to the other two types, the orthorhombic $NiSe_2$ NCs were more metallic and formed fewer surface oxides, which increased the photocurrent and transfer onset potential, resulting in better photoelectrocatalytic performance and exerted efficient water-splitting ability.

Nickel hydroxide and hydroxyl oxides

Among the nickel-based materials that catalyze OER, nickel hydroxide and its hydroxyl oxides (collectively

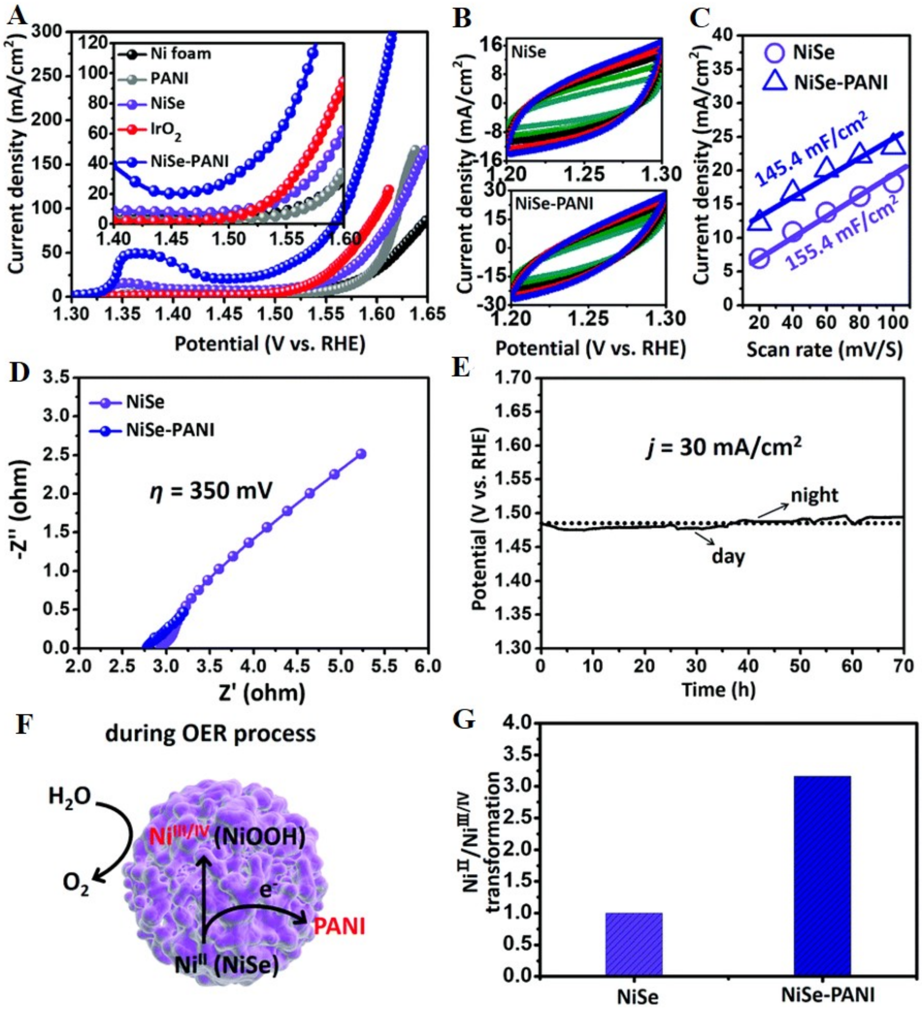

Figure 10. OER electrocatalytic performance. (A) LSV curves for OER of blank Ni foam, PANI, NiSe, commercial IrO_2 deposited on Ni foam (~1 mg·cm^{-2}) and NiSe-PANI. (B) Cyclic voltammograms of NiSe and NiSe-PANI at different scan rates (from 20 to 100 mV·s^{-1} with an increment of 20 mV·s^{-1}). (C) Scan rate dependence of current densities for NiSe and NiSe-PANI at 1.25 V vs. RHE. (D) Nyquist plots of NiSe and NiSe-PANI at η of 350 mV. (E) Chronopotentiometric curves of NiSe-PANI at j of 30 mA·cm^{-2} for a continuous OER process. (F) Schematic mechanism of NiSe-PANI for an efficient OER. The enhanced generation of NiIII/IV active species when oxidized promotes the OER process. (G) Normalized transformation of NiII to NiIII/IV on the basis of NiSe, revealing the enhanced generation of NiIII/IV due to PANI functionalization. Reproduced with permission. Copyright 2018, Royal Society of Chemistry[108].

referred to as NiOx) are a class of electrocatalytic materials with excellent application prospects[111]. Since the sluggish kinetics of the OER are the main limitations of the performance of hydrogen production from electrolytic water, improving the catalytic performance of NiOx on the OER has been the focus of major research[112]. In order to better understand the effect of NiOx species on the catalytic performance of the OER, it is very important to analyze the structural and phase changes in the water oxidation reaction. Luan *et al.*[113] synthesized a 2D-$Ni(OH)_2$ catalytic material by a layered reverse micelle method because the 2D-$Ni(OH)_2$ phase could be formed at an anodic potential γ-NiOOH active phase, thus showing better OER catalytic activity and stability. Gao *et al.*[114] controllably prepared α-$Ni(OH)_2$ and β-$Ni(OH)_2$ by a solvothermal system and compared their OER catalytic activities. The results indicated that α-$Ni(OH)_2$ than β-$Ni(OH)_2$ presented better OER activity and higher stability [Figure 11], which was mainly due to the formation of γ-NiOOH through α-$Ni(OH)_2$, thus promoting the diffusion of OER intermediates and the corresponding conversion to O_2. After characterizing and analyzing the surface morphology of α-$Ni(OH)_2$

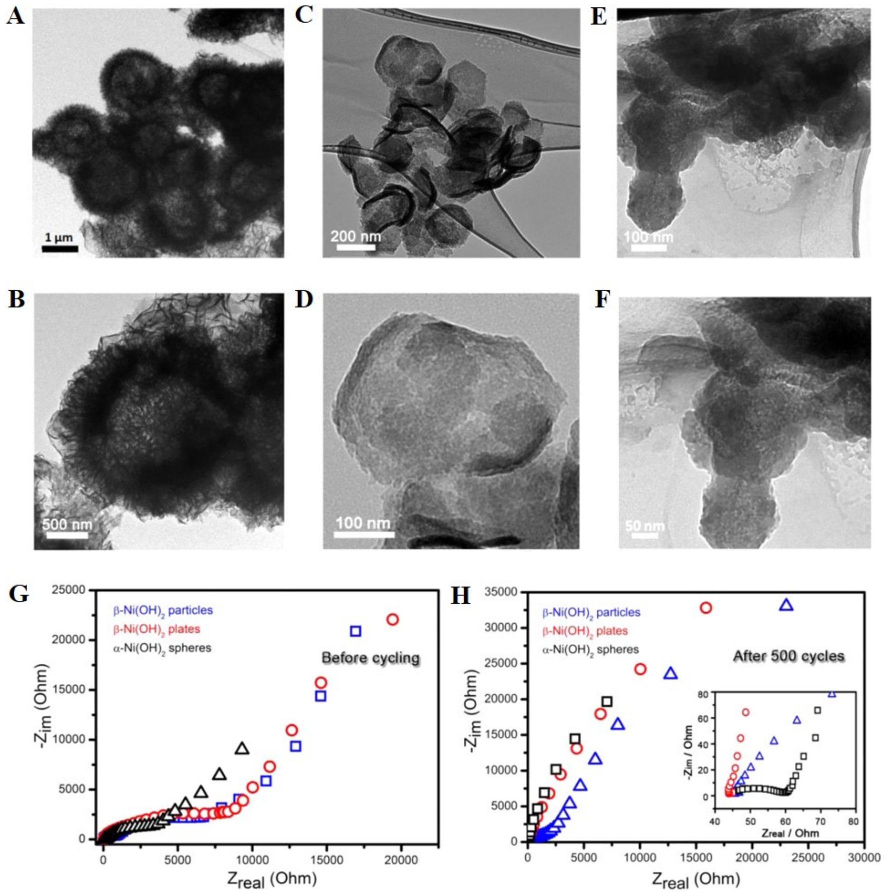

Figure 11. TEM and HRTEM images taken after 500 cycles for α-$Ni(OH)_2$ hollow spheres (A, B), β-$Ni(OH)_2$ nanoplates (C, D) and β-$Ni(OH)_2$ nanoparticles (E, F). EIS Nyquist plots of α- and β-$Ni(OH)_2$ nanocrystals before (G) and after (H) 500 cycles. Inset in panel h shows the corresponding Nyquist plot at the high-frequency range. Reproduced with permission. Copyright 2018, American Chemical Society[113].

and β-$Ni(OH)_2$ for 500 CV cycles by TEM, it was demonstrated that the α-$Ni(OH)_2$ phase could be easily transformed into γ-NiOOH without material expansion or mechanical deformation, whereas for β-$Ni(OH)_2$, a large number of nanoparticles were observed to accumulate and the surface was severely corroded after CV cycling, manifesting that β-$Ni(OH)_2$ had weak structural stability during the OER process due to Jahn-Teller distortion (spontaneous symmetry break in solid-state system) at the low spin d^7 Ni^{3+} center. Similarly, Dou *et al.*[111] compared the OER activities of only γ-NiOOH with both containing γ-NiOOH and β-NiOOH. It was found that the electrocatalytic activity of γ-NiOOH for OER was much higher than that of NiOOH mixed with γ- and β-phases. The high OER electrochemical activity of γ-NiOOH phase was attributed to its large layer spacing, which facilitated the diffusion of electrolytes and the desorption of O_2 molecules on the electrocatalyst surface.

Combined with the above discussion on the OER activities of β-NiOOH and γ-NiOOH, Li *et al.*[115] directly confirmed that the OER catalytic activity of γ-NiOOH was better than β-NiOOH. Nevertheless, γ-NiOOH or β-NiOOH with high activity on OER was still controversial. Some research has elucidated that γ-NiOOH is the active center of the OER, while other researchers have claimed that β-NiOOH is the active center of the OER. Therefore, all these contradictory studies on NiOx active centers illustrate that, in addition to the active phase, the OER activity of NiOx electrocatalyst also depends on its preparation method, initial precursor (mainly containing trace transition metal impurities, such as Fe, Ce, Cd, Pb and Zn), electrode cycle, morphology, active surface area and electrolyte[116,117]. More specifically, Corrigan *et al*.[116] found that the inclusion of Fe into the $Ni(OH)_2$ could significantly accelerate OER kinetics, while doping other transition metal elements, such as Cd, Pb and Zn, hindered the catalytic performance of the OER. According to the experimental observation, the significant effect of Fe on the OER activity of $Ni(OH)_2$ was mainly associated with the change of electrocatalyst conductivity and the formation of the active center, which was more favorable to catalyzing OER intermediates. Correspondingly, Trotochaud *et al*.[117] detected Fe impurities in NiOOH from an analytical grade KOH solution. They found that the presence of a small amount of Fe impurities in NiOOH could significantly promote the OER activity, while NiOOH exhibited inferior OER activity in a Fe-free KOH electrolyte (raw KOH was completely purified from Fe impurities).

Many theoretical and experimental groups have researched the role of Fe into $Ni(OH)_2$ and NiOOH for the OER activity to judge whether Fe itself acts as the active center or just activated $Ni(OH)_2$ and NiOOH to obtain better OER performance[118]. Friebel *et al*.[119] carried out DFT calculations of the OER on γ-NiOOH and Fe-doped γ-NiOOH. The results demonstrated that the overpotential of Fe-doped γ-NiOOH to the OER (0.43 V) was much lower than that of γ-NiOOH (0.56V) and Fe in $Ni_{1-x}Fe_xOOH$ was the active center of the OER. In addition, the effect of Fe on the structure of $Ni(OH)_2$/NiOOH electrocatalyst was investigated by EXAFS characterization. The results concluded that the addition of Fe did not change the Ni-O bond length but the Fe-O bond length exhibited an obvious shrinkage in the oxidation of $Ni_{1-x}Fe_x$ OOH, which optimized the binding adsorption energy of OER intermediates and reduced the OER overpotential. Wu *et al*.[120] compared the OER catalytic activities of NiO/NF and Fe-doped NiO/NF ($Fe_{11\%}$-NiO/NF). The results presented that $Fe_{11\%}$-NiO/NF had better OER electrocatalytic performance and higher stability than NiO/NF. The Fe doping of $Fe_{11\%}$-NiO/NF electrocatalyst and its mesoporous structure was mainly responsible for the excellent OER catalytic performance [Figure 12]. Among them, the mesoporous NS structure of NF provided rich open space for facilitating the diffusion of electrolytes and the close contact between electrolytes and electrocatalysts. More importantly, Fe doping reduced the energy barrier of molecular oxygen generated by OER intermediates.

Li *et al*.[121] compared the OER activities of NiFe-LDH and Ni $(OH)_2$NS electrocatalysts. The results showed that the OER activity of NiFe-LDH was smaller than that of $Ni(OH)_2$ NSs. Furthermore, they also researched the effect of vanadium doping into the NiFe LDH (NiFeV-LDH) electrocatalyst on OER activity. The results disclosed that NiFeV-LDHs delivered high OER catalytic activity and stability. The result was attributed to the reason that the electronic structure of the whole electrocatalyst was changed by vanadium doping, which improved its conductivity and the number of catalytic active sites. Li *et al*.[122] deposited double oxygen evolution catalyst (OEC) layers (FeOOH and NiOOH) over the nanotube array-like WO_3 (WA) surface to form a WA-OEC photoanode. Therein, FeOOH greatly reduced the WA/OEC interface electron-hole pairs recombination rate, while NiOOH restricted the recombination of electron-hole pairs at the OEC/electrolyte interface and significantly improved the corresponding OER activity. The WA/OEC photoanode had a photocurrent density of 120 $\mu A \cdot cm^{-2}$ under simulated sunlight illumination, showing a good photoelectrocatalytic water-splitting efficiency. Wei *et al*.[123] composited NiOOH with CdS as a photoelectrocatalyst (CdS/NiOOH). After a 3600 s photoelectrocatalytic stability test, the stability of CdS/NiOOH was significantly improved by 44.50% compared with pure CdS due to NiOOH preventing the oxidation of CdS by trapping photogenerated holes. Furthermore, the deposition of NiOOH was more beneficial in accelerating the separation of photogenerated carriers, thereby enhancing the photoelectrocatalytic activity for the water-splitting process. Pirkarami *et al*.[124] synthesized a novel 3D CdS@NiCo-LDH material as a cost-effective, bifunctional and efficient photoelectrocatalyst for water splitting, which had the advantages of high specific surface area, fast electron transfer and multiple channels

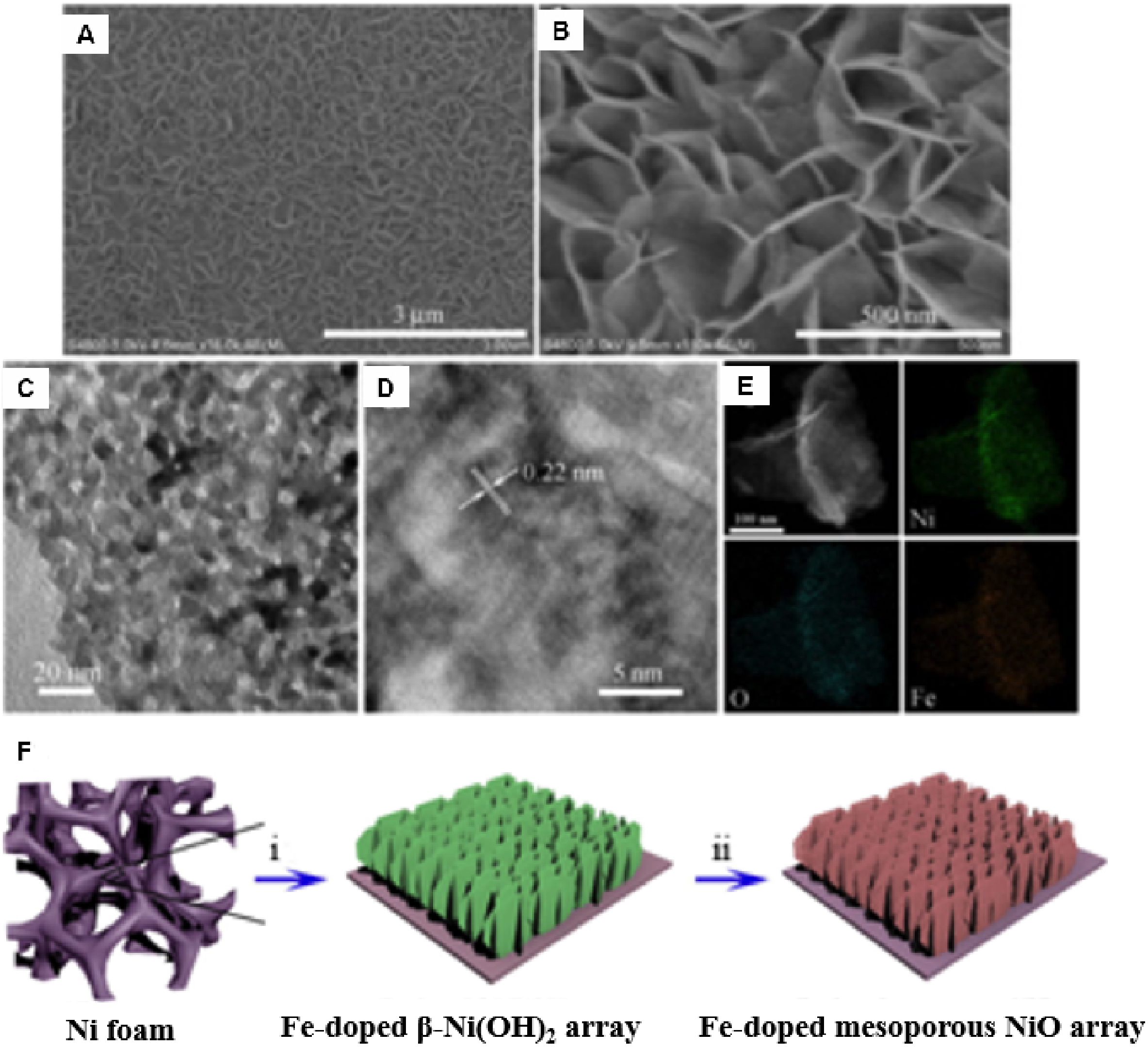

Figure 12. Morphological and structural characterization of $Fe_{11\%}$-NiO/NF. (A, B) FESEM images with low and high magnification. (C) TEM image of mesoporous nanosheet. (D) HRTEM image of mesoporous nanosheet. (E) STEM image of mesoporous NS and corresponding elemental mapping images. (F) Graphical representation of formation process of Fe-doped NiO mesoporous NS array. (i) Solvothermal deposition of Fe-doped β-$Ni(OH)_2$ NS array precursor on Ni foam. (ii) Fe-doped NiO mesoporous NS array on Ni foam by calcination Fe-doped β-$Ni(OH)_2$ NS array precursor in air. Reproduced with permission. Copyright 2017, Elsevier[120].

to release gaseous products, resulting in better electrocatalytic OER activity in alkaline environments. When using this electrocatalyst for the HER, it could achieve current density values of 10 and 100 mA·cm^{-2} at voltages of 379 and 202 mV, respectively.

Nickel is the fourth largest metal element in terms of reserves and has the same main group as platinum with high electrocatalytic activity. Therefore, research into Ni-based materials as HER electrocatalysts has proved both popular and fruitful[125]. For example, Zhang *et al.*[126] successfully prepared $NiCo_2P_x$ nanowires (NWs) and after conducting characterization and performing experiments, concluded that for the HER in 1.0 M KOH, the $NiCo_2P_x$NWs delivered negligible attenuation at 250 mA·cm^{-2} after 5000 CV cycles, indicating reasonably high durability. They also showed relatively high HER activity (η = 58 mV at 10 mA·cm^{-2}) and negligible attenuation at 30 h under an overpotential of η = 100 mV, indicating its ultralong stability [Figure 13]. Li *et al.*[127] obtained porous sea urchin-like $Ni_{0.5}Co_{0.5}P$ by the combination of calcinating and phosphating treatment of $NiCo(CO_3)(OH)_2$ in an Ar atmosphere. For the HER in 1.0 M KOH, the electrocatalyst presented negligible attenuation after 1000 CV cycles, indicating its high durability and activity for the HER (η of 87 mV at 10 mA·cm^{-2}). Wang *et al.*[128] synthesized a Ni-reduced GO (rGO) nanostructure using an electrodeposition strategy in a supergravity field. Benefiting from its high surface area, good electrical conductivity and synergistic effect between Ni nanoparticles and rGO sheets, the Ni-rGO exhibited reasonable stability at 250/100 mA·cm^{-2} for the HER during a durability test in 1.0 M NaOH. It also showed excellent HER activity (η of 36 mV at 10 mA·cm^{-2}). Similarly, Ni/C_3N_4 nanostructured composites prepared by electrodeposition under a supergravity field could also improve the stability and activity for the HER. Wang *et al.*[129] reported that nanostructured Ni/C_3N_4 exhibited high stability and activity for the HER in 1.0 M NaOH. More specifically, the Ni/C_3N_4 presented high HER activity (η of 222 mV at 10 mA·cm^{-2}) and negligible attenuation at 100 mA·cm^{-2} within 12 h.

In addition, like iron, nickel phosphide and sulfide also have good HER electrocatalytic activity. For example, Wang *et al.*[130] prepared $Ni(OH)_2$•$0.75H_2O$ by a hydrothermal method and then phosphated the nanostructured Ni_5P_4 in a N_2 atmosphere at 370 °C. The electrocatalyst exhibited high conductivity, which significantly enhanced its high activity and stability for the HER. For the HER in 1.0 M KOH, Ni_5P_4 showed negligible decay after 3600 CV cycles, indicating its very high durability and HER activity (η of 47 mV at 10 mA·cm^{-2}). Wang *et al.*[131] reported that the high HER activity of Ni_xP_y could be achieved by simply growing in 3D-NF. 3D-NF had a porous layered structure and large specific surface area, which significantly reduced the diffusion path length of ions and improved the electron and ion conductivity in the HER process. In addition, Lado *et al.*[132] found that Al-doped Ni-P (AlNiP) provided higher HER catalytic activity (η_{10} = 111 mV) than pure NiP (η_{10} = 175 mV). This indicated that the doping of Al changed the state density of NiP to reduce the energy barrier of the HER dynamics.

Tong *et al.*[133] prepared Ni_3S_2 by a hydrothermal method and showed that Ni_3S_2 nanorods@Ni_3S_2 NSs exhibited higher HER activity than Ni_3S_2 nanorods. Ni_3S_2 formed by a nanorod@nanosheet homojunction can provide abundant active sites to reduce electron transport and promote gas release, which might enhance its high durability and activity for the HER [Figure 14]. For the HER in 1.0 M KOH, Ni_3S_2 showed negligible attenuation after 10,000 CV cycles, indicating very high durability, it also delivered very high HER activity (η of 48.1 mV at 10 mA·cm^{-2}) and reasonable stability at 48 mV for 24 h. Yang *et al.*[134] first fabricated nanoporous Cu by electrodeposition and etching and finally prepared nanoporous Ni_3S_2@Cu by an electrodisplacement strategy. The porous structure of the electrocatalyst provided a large number of active sites, which enhanced its catalytic activity and durability for the HER. For the HER in 1.0 M KOH, the Ni_3S_2@Cu activated catalyst exhibited negligible decay at 200 mA·cm^{-2} after 2000 CV cycles, which indicated its much high durability, and much higher HER activity (η of 60.8 mV at 10 mA·cm^{-2}). In addition, Long *et al.*[135] synthesized Fe-Ni ultrathin NSs as an acidic HER electrocatalyst, which exhibited excellent HER activity (η_{10} = 105 mV and ζ = 40 mV dec^{-1}) and high stability. Qu *et al.*[136] developed vanadium-doped Ni_3S_2NW on NF, which presented good stability of η_{10} = 68 mV and 8000 CV cycles in alkaline solution. In addition, Wang *et al.*[137] synthesized a platinum nickel/nickel sulfide nanowire (Pt_3Ni/NiS nanowire) as a HER electrocatalyst, which displayed j = 37.2 mA·cm^{-2} in η = 70 mV in a 1 M KOH solution, 9.7 times better than 20% Pt/C.

It is precisely because these transition metals (Fe, Co and Ni) have the advantages of low expenditure, chemical stability, unique and adjustable electronic structure, rich redox states and high intrinsic activity that they are not only regarded as the best potential alternatives to replace traditional noble-metal-contained

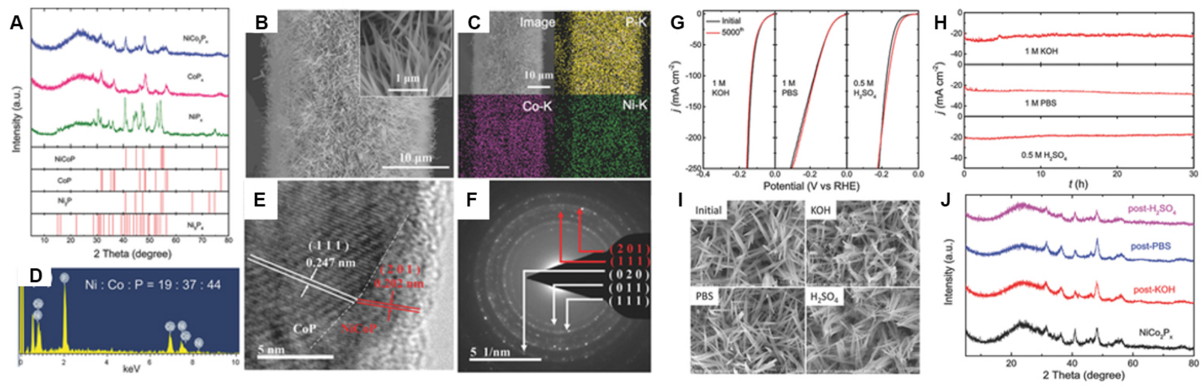

Figure 13. Structural characterization of as-obtained phosphides. (A) XRD patterns of NiPx, CoPx and $NiCo_2P_x$. (B) SEM images. (C) Elemental mapping of P, Co, and Ni. (D) EDX spectrum. (E) HRTEM image. (F) Corresponding SAED pattern of $NiCo_2P_x$. HER stabilities of $NiCo_2P_x$. (G) Polarization curves for $NiCo_2P_x$ before and after 5000 cycles with a scan rate of 100 mV s^{-1} between +0.20 and -0.20 V. (H) Time dependence of current density for $NiCo_2P_x$ at static overpotentials of 100 mV (in 1 M KOH and PBS) and 150 mV (in 0.5 M H_2SO_4) for 30 h. (I) SEM images and (J) XRD patterns of $NiCo_2P_x$ NWs before and after long-time test. Reproduced with permission. Copyright 2017, Wiley[126].

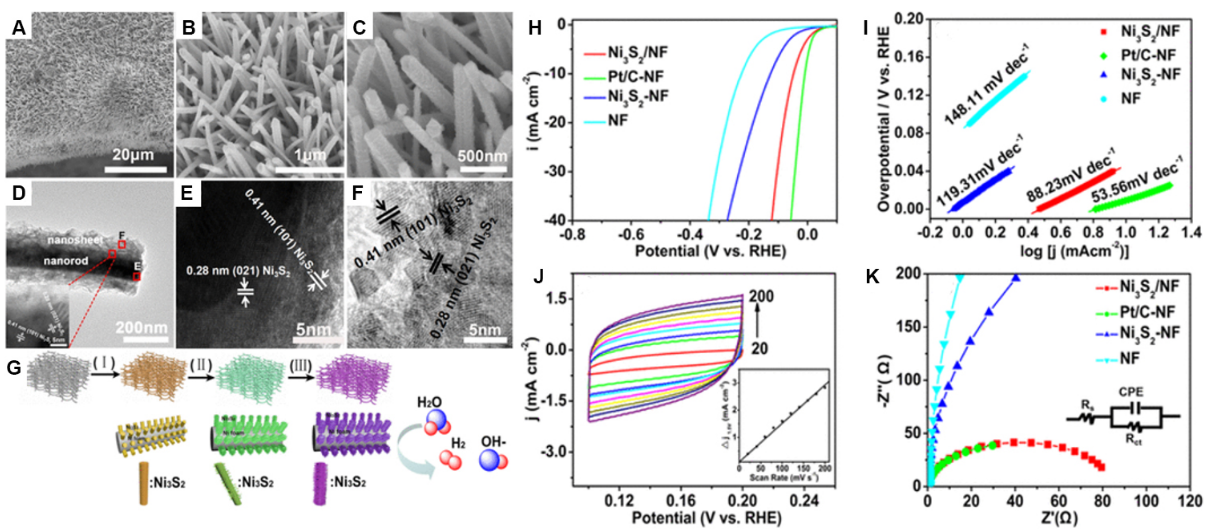

Figure 14. (A-C) SEM, d) TEM and (E, F) corresponding HRTEM images of enlarged red frame area from (D) for Ni_3S_2/NF. (G) Proposed formation mechanism of Ni_3S_2/NF. (H) LSV curves at a scan rate of 5 mV s^{-1} with iR correction. (I) Corresponding Tafel plots of Ni_3S_2/NF, Ni_3S_2-NF, Pt/C-NF and NF. (J) CV curves of Ni_3S_2/NF at different scanning rates of 20-200 mV s^{-1} in the potential window of 0.1-0.2 V (inset: linear fitting of the capacitive currents obtained at 0.15 V). (K) EIS Nyquist fitting plots of Ni_3S_2/NF, Ni_3S_2-NF, Pt/C-NF and NF at the open-circuit potential with an amplitude of 5 mV, inset is the corresponding equivalent circle for fitting. Reproduced with permission. Copyright 2017, American Chemical Society[133].

OER/HER electrocatalysts but can also be used as energy storage materials in the field of clean energy, such as lithium-ion batteries, fuel cells and supercapacitors[138]. Although some important research progress has been made in the preparation and theory of these metals and some matrix materials as functional materials, there still exist several problems to be resolved. On the one hand, due to the facile aggregation characteristics of these nanomaterials, the exposed quantity and quality of functional active sites are undesirable. On the other hand, due to the characteristics of the metastable structure of quantum-level nanomaterials, their structures were vulnerable to structural collapse and agglomeration. These phenomena could easily cause the functional exposed active sites to be covered and inactivated. Therefore, it still remained a big challenge to resolve the high-quality and high-density active site exposure and structural stabilities of these materials employed in these fields.

CONCLUSION AND OUTLOOK

The water-splitting electrolyzer is regarded as a promising technology for dissociating water into high-purity hydrogen in a low-expenditure, zero-pollution emission and high-efficiency manner. Potential strategies for designing the earth-abundant first-row transition metal (Fe, Co and Ni)-based composite materials as electrocatalysts to substitute noble-metal-based electrocatalysts have been profoundly discussed in this review. Noticeably, the recently developed catalysts of these categories have exhibited excellent OER electrocatalytic activities, which are comparable or superior to precious-metal-based electrocatalysts (Ru, Ir, RuO_2 and IrO_2). Moreover, the influence of morphologies, compositions and heteroatom doping on the OER kinetics have been described. Highly efficient electrocatalysts made of Fe and Ni-based compositions are also extensively applicable to the field of the HER and have been elaborated in a short separate section, which differentiates the strategy in making good Fe and Ni HER electrocatalysts from the OER, demonstrating the wide applicability of these Fe and Ni-based nanocomposites. Nevertheless, the fabrication of high-performance water-splitting electrocatalysts remains at a preliminary stage and future works are needed to continue to develop novel high-performance OER electrocatalysts.

Realistically, there are some investigations illustrating that transition metal nitride nanomaterials are regarded as the best potential materials to replace traditional noble metal-based electrocatalysts because of their low-expenditure, chemical stability, unique and adjustable electronic structure, rich redox states and high electrocatalytic intrinsic activity. In this regard, the selection of appropriate precursors is an important prerequisite for the design and optimization of transition metal nitride electrocatalyst synthesis routes. Nitrogen-containing polymers (NCPs) are considered as appropriate precursors for the preparation of transition metal nitride. This is because NCPs can effectively coordinate with transition metal ions (TMI) to form a strong TM-N bond, which is more conducive to strengthening the anchoring and dispersion of transition metal ions. Therefore, M/NCP precursors prepared by impregnation methods (M = Fe, Co or Ni) can convert TM-N bonds into M-N-C bonds in MN_x/C under high-temperature carbonization treatment. The active site of this nanostructure not only has high stability and corrosion resistance under alkaline conditions, but also has high OER intrinsic catalytic activity. MN_x/CN electrocatalyst carbonized from M/NCP precursor exhibits high conductivity, so it strengthens the electrical transfer capability of OER process. Therefore, rendering NCPs as C and N sources to prepare MN_x/CN electrocatalysts with different metal coordination environments by controlling carbonization temperature and metal loading has become an important means to obtain efficient OER electrocatalysts. Furthermore, NCPs can be used as precursors to prepare high-density M-N-C single-atom electrocatalyst. The electrocatalyst with this structure can not only fully improve the atomic utilization efficiency of metal but also exposes the active sites of metal to the greatest extent and promote the occurrence of catalyzing the OER. In addition, a single regular M-N-C single-atom electrocatalyst is helpful to reveal the “structure-activity” relationship between its active site structure and OER electrocatalytic activity. Furthermore, NCPs can also serve as precursors to preparing high-dispersed supported bimetallic electrocatalysts. The synergistic effect between metals can adjust the electronic state of the electrocatalyst surface, as well as simultaneously helping to strengthen the adsorption energy of OER intermediate species, so as to improve the integrated electrochemical performance of the OER.

DECLARATIONS

Authors’ contributions

Conceived the manuscript: Chen X, Liu J

Wrote the manuscript: Chen X, Yuan T, Zhang Z
Reviewed the manuscript: Gao X, Wang N, Cui L
Contributed to the discussion of the manuscript: Chen X, Song C, Yang S, Cui L

Availability of data and materials
Not applicable.

Financial support and sponsorship
This work was financially supported by the National Natural Science Foundation of China (Grant No. 21804008, 52102209) acquired by co-authors Lifeng Cui and Nannan Wang, the International Technological Collaboration Project of Shanghai (Grant No. 17520710300) acquired by co-author Lifeng Cui, and Anhui Provincial Natural Science Foundation (Grant No. 2108085QE197) acquired by co-author Nannan Wang, and Guangdong Basic and Applied Basic Research Foundation (Grant No. 2022A1515010834, 2020A1515110221) acquired by co-authors Xiaodong Chen and Nannan Wang.

Conflicts of interest
All authors declared that there are no conflicts of interest.

Ethical approval and consent to participate
Not applicable.

Consent for publication
Not applicable.

REFERENCES

1. Dingbang C, Cang C, Qing C, Lili S, Caiyun C. Does new energy consumption conducive to controlling fossil energy consumption and carbon emissions? *Resour Policy* 2021;74:102427. DOI
2. Pirgaip B, Dinçergök B. Economic policy uncertainty, energy consumption and carbon emissions in G7 countries: evidence from a panel Granger causality analysis. *Environ Sci Pollut Res Int* 2020;27:30050-66. DOI PubMed
3. Chang Z, Yu F, Liu Z, et al. Co-Ni Alloy Encapsulated by N-doped graphene as a cathode catalyst for rechargeable hybrid Li-air batteries. *ACS Appl Mater Interfaces* 2020;12:4366-72. DOI PubMed
4. Yu N, Wu C, Huang W, et al. Highly efficient Co_3O_4/Co@NCs bifunctional oxygen electrocatalysts for long life rechargeable Zn-air batteries. *Nano Energy* 2020;77:105200. DOI
5. Zeng F, Mebrahtu C, Liao L, Beine AK, Palkovits R. Stability and deactivation of OER electrocatalysts: a review. *J Energy Chem* 2022;69:301-29. DOI
6. Adams S, Adedoyin F, Olaniran E, Bekun FV. Energy consumption, economic policy uncertainty and carbon emissions; causality evidence from resource rich economies. *Econ Anal Policy* 2020;68:179-90. DOI PubMed
7. Johnsson F, Kjärstad J, Rootzén J. The threat to climate change mitigation posed by the abundance of fossil fuels. *Clim Policy* 2019;19:258-74. DOI
8. Yang C, Gao N, Wang X, et al. Phosphate boosting stable efficient seawater splitting on porous NiFe (oxy)hydroxide@$NiMoO_4$ Core-Shell micropillar electrode. *Energy Mater* 2021;1:100015. DOI
9. Nazir MS, Ali ZM, Bilal M, Sohail HM, Iqbal HMN. Environmental impacts and risk factors of renewable energy paradigm-a review. *Environ Sci Pollut Res Int* 2020;27:33516-26. DOI PubMed
10. Chen B, Xiong R, Li H, Sun Q, Yang J. Pathways for sustainable energy transition. *J Clean Prod* 2019;228:1564-71. DOI
11. Liu J, Chen Z, Koh MJ, Loh KP. Deuterium labelling by electrochemical splitting of heavy water. *Energy Mater* 2021;1:100016. DOI
12. Jin X, Li X, Lei H, et al. Comparing electrocatalytic hydrogen and oxygen evolution activities of first-row transition metal complexes with similar coordination environments. *J Energy Chem* 2021;63:659-66. DOI
13. El-emam RS, Özcan H. Comprehensive review on the techno-economics of sustainable large-scale clean hydrogen production. *J Clean Prod* 2019;220:593-609. DOI

14. Yu M, Wang K, Vredenburg H. Insights into low-carbon hydrogen production methods: green, blue and aqua hydrogen. *Int J Hydrog Energy* 2021;46:21261-73. DOI
15. Seh ZW, Kibsgaard J, Dickens CF, Chorkendorff I, Nørskov JK, Jaramillo TF. Combining theory and experiment in electrocatalysis: insights into materials design. *Science* 2017;355:eaad4998. DOI PubMed
16. Hunter BM, Gray HB, Müller AM. Earth-abundant heterogeneous water oxidation catalysts. *Chem Rev* 2016;116:14120-36. DOI PubMed
17. Suen NT, Hung SF, Quan Q, Zhang N, Xu YJ, Chen HM. Electrocatalysis for the oxygen evolution reaction: recent development and future perspectives. *Chem Soc Rev* 2017;46:337-65. DOI PubMed
18. Hu C, Dai L. Carbon-based metal-free catalysts for electrocatalysis beyond the ORR. *Angew Chem Int Ed Engl* 2016;55:11736-58. DOI PubMed
19. Zhang W, Lai W, Cao R. Energy-related small molecule activation reactions: oxygen reduction and hydrogen and oxygen evolution reactions catalyzed by porphyrin- and corrole-based systems. *Chem Rev* 2017;117:3717-97. DOI PubMed
20. Jia Y, Zhang L, Gao G, et al. A heterostructure coupling of exfoliated Ni-Fe hydroxide nanosheet and defective graphene as a bifunctional electrocatalyst for overall water splitting. *Adv Mater* 2017;29:1700017. DOI PubMed
21. Long X, Li J, Xiao S, et al. A strongly coupled graphene and FeNi double hydroxide hybrid as an excellent electrocatalyst for the oxygen evolution reaction. *Angew Chem Int Ed Engl* 2014;53:7584-8. DOI PubMed
22. Fan K, Chen H, Ji Y, et al. Nickel-vanadium monolayer double hydroxide for efficient electrochemical water oxidation. *Nat Commun* 2016;7:11981. DOI PubMed PMC
23. Zhou LJ, Huang X, Chen H, Jin P, Li GD, Zou X. A high surface area flower-like Ni-Fe layered double hydroxide for electrocatalytic water oxidation reaction. *Dalton Trans* 2015;44:11592-600. DOI PubMed
24. Feng LL, Yu G, Wu Y, et al. High-index faceted Ni_3S_2 nanosheet arrays as highly active and ultrastable electrocatalysts for water splitting. *J Am Chem Soc* 2015;137:14023-6. DOI PubMed
25. Zhao W, Zhang C, Geng F, Zhuo S, Zhang B. Nanoporous hollow transition metal chalcogenide nanosheets synthesized via the anion-exchange reaction of metal hydroxides with chalcogenide ions. *ACS Nano* 2014;8:10909-19. DOI PubMed
26. Li K, Zhang J, Wu R, Yu Y, Zhang B. Anchoring CoO domains on $CoSe_2$ nanobelts as bifunctional electrocatalysts for overall water splitting in neutral media. *Adv Sci (Weinh)* 2016;3:1500426. DOI PubMed PMC
27. Xu R, Wu R, Shi Y, Zhang J, Zhang B. Ni_3Se_2 nanoforest/Ni foam as a hydrophilic, metallic, and self-supported bifunctional electrocatalyst for both H_2 and O_2 generations. *Nano Energy* 2016;24:103-10. DOI
28. Jia X, Zhao Y, Chen G, et al. Water splitting: Ni_3FeN nanoparticles derived from ultrathin NiFe-layered double hydroxide nanosheets: an efficient overall water splitting electrocatalyst (Adv. Energy Mater. 10/2016). *Adv Energy Mater* 2016:6. DOI
29. Thiyagarajan D, Gao M, Sun L, et al. Nanoarchitectured porous Cu-CoP nanoplates as electrocatalysts for efficient oxygen evolution reaction. *Chem Eng J* 2022;432:134303. DOI
30. Zhang C, Huang Y, Yu Y, Zhang J, Zhuo S, Zhang B. Sub-1.1 nm ultrathin porous CoP nanosheets with dominant reactive {200} facets: a high mass activity and efficient electrocatalyst for the hydrogen evolution reaction. *Chem Sci* 2017;8:2769-75. DOI PubMed PMC
31. Wang X, Li W, Xiong D, Petrovykh DY, Liu L. Bifunctional nickel phosphide nanocatalysts supported on carbon fiber paper for highly efficient and stable overall water splitting. *Adv Funct Mater* 2016;26:4067-77. DOI
32. Chen J, Zheng F, Zhang S, et al. Interfacial interaction between FeOOH and Ni-Fe LDH to modulate the local electronic structure for enhanced OER electrocatalysis. *ACS Catal* 2018;8:11342-51. DOI
33. Zhou P, He J, Zou Y, et al. Single-crystalline layered double hydroxides with rich defects and hierarchical structure by mild reduction for enhancing the oxygen evolution reaction. *Sci China Chem* 2019;62:1365-70. DOI
34. Kim YT, Lopes PP, Park SA, et al. Balancing activity, stability and conductivity of nanoporous core-shell iridium/iridium oxide oxygen evolution catalysts. *Nat Commun* 2017;8:1449. DOI PubMed PMC
35. Hu C, Zhang L, Gong J. Recent progress made in the mechanism comprehension and design of electrocatalysts for alkaline water splitting. *Energy Environ Sci* 2019;12:2620-45. DOI
36. Shi Q, Zhu C, Du D, Lin Y. Robust noble metal-based electrocatalysts for oxygen evolution reaction. *Chem Soc Rev* 2019;48:3181-92. DOI PubMed
37. Owe L, Tsypkin M, Wallwork KS, Haverkamp RG, Sunde S. Iridium-ruthenium single phase mixed oxides for oxygen evolution: Composition dependence of electrocatalytic activity. *Electrochim Acta* 2012;70:158-64. DOI
38. Lv L, Yang Z, Chen K, Wang C, Xiong Y. Electrocatalysts: 2D layered double hydroxides for oxygen evolution reaction: from fundamental design to application (Adv. Energy Mater. 17/2019). *Adv Energy Mater* 2019;9:1970057. DOI
39. Zhang J, Zhang Q, Feng X. Support and interface effects in water-splitting electrocatalysts. *Adv Mater* 2019;31:e1808167. DOI PubMed
40. Bian W, Huang Y, Xu X, Ud Din MA, Xie G, Wang X. Iron hydroxide-modified nickel hydroxylphosphate single-wall nanotubes as efficient electrocatalysts for oxygen evolution reactions. *ACS Appl Mater Interfaces* 2018;10:9407-14. DOI PubMed
41. Liu K, Zhang C, Sun Y, et al. High-performance transition metal phosphide alloy catalyst for oxygen evolution reaction. *ACS Nano* 2018;12:158-67. DOI PubMed
42. Dutta A, Mutyala S, Samantara AK, Bera S, Jena BK, Pradhan N. Synergistic effect of inactive iron oxide core on active nickel phosphide shell for significant enhancement in oxygen evolution reaction activity. *ACS Energy Lett* 2018;3:141-8. DOI

43. Zhang J, Liu J, Xi L, et al. Single-atom Au/NiFe layered double hydroxide electrocatalyst: probing the origin of activity for oxygen evolution reaction. *J Am Chem Soc* 2018;140:3876-9. DOI PubMed
44. Sun F, Li L, Wang G, Lin Y. Iron incorporation affecting the structure and boosting catalytic activity of β-$Co(OH)_2$: exploring the reaction mechanism of ultrathin two-dimensional carbon-free Fe_3O_4 -decorated β-$Co(OH)_2$ nanosheets as efficient oxygen evolution electrocatalysts. *J Mater Chem A* 2017;5:6849-59. DOI
45. Feng JX, Xu H, Dong YT, Ye SH, Tong YX, Li GR. FeOOH/Co/FeOOH hybrid nanotube arrays as high-performance electrocatalysts for the oxygen evolution reaction. *Angew Chem Int Ed Engl* 2016;55:3694-8. DOI PubMed
46. Zhang B, Zheng X, Voznyy O, et al. Homogeneously dispersed multimetal oxygen-evolving catalysts. *Science* 2016;352:333-7. DOI PubMed
47. Zhang L, Meng T, Mao B, Guo D, Qin J, Cao M. Multifunctional Prussian blue analogous@polyaniline core-shell nanocubes for lithium storage and overall water splitting. *RSC Adv* 2017;7:50812-21. DOI
48. Zhang J, Zhang M, Qiu L, et al. Three-dimensional interconnected core-shell networks with Ni(Fe)OOH and M-N-C active species together as high-efficiency oxygen catalysts for rechargeable Zn-air batteries. *J Mater Chem A* 2019;7:19045-59. DOI
49. Dong Y, Feng J, Li G. Correction to transition metal ion-induced high electrocatalytic performance of conducting polymer for oxygen and hydrogen evolution reactions. *Macromol Chem Phys* 2019;220:1900525. DOI
50. Liu B, Peng HQ, Ho CN, et al. Mesoporous nanosheet networked hybrids of cobalt oxide and cobalt phosphate for efficient electrochemical and photoelectrochemical oxygen evolution. *Small* 2017;13:1701875. DOI PubMed
51. Yang Z, Zhao L, Zhang S, Zhao X. Ferroelectric-enhanced $BiVO_4$-$BiFeO_3$ photoelectrocatalysis for efficient, stable and large-current-density oxygen evolution. *Appl Mater Today* 2022;26:101374. DOI
52. Zhu Y, Zhao X, Li J, et al. Surface modification of hematite photoanode by NiFe layered double hydroxide for boosting photoelectrocatalytic water oxidation. *J Alloys Compd* 2018;764:341-6. DOI
53. Xu X, Song F, Hu X. A nickel iron diselenide-derived efficient oxygen-evolution catalyst. *Nat Commun* 2016;7:12324. DOI PubMed PMC
54. Hung S, Hsu Y, Chang C, et al. Unraveling geometrical site confinement in highly efficient iron-doped electrocatalysts toward oxygen evolution reaction. *Adv Energy Mater* 2018;8:1701686. DOI
55. Zhuang L, Ge L, Yang Y, et al. Ultrathin iron-cobalt oxide nanosheets with abundant oxygen vacancies for the oxygen evolution reaction. *Adv Mater* 2017;29:1606793. DOI PubMed
56. Jin Y, Huang S, Yue X, Du H, Shen PK. Mo- and Fe-modified $Ni(OH)_2$/NiOOH nanosheets as highly active and stable electrocatalysts for oxygen evolution reaction. *ACS Catal* 2018;8:2359-63. DOI
57. Yu F, Zhou H, Zhu Z, et al. Three-dimensional nanoporous iron nitride film as an efficient electrocatalyst for water oxidation. *ACS Catal* 2017;7:2052-7. DOI
58. Yang Y, Lun Z, Xia G, Zheng F, He M, Chen Q. Non-precious alloy encapsulated in nitrogen-doped graphene layers derived from MOFs as an active and durable hydrogen evolution reaction catalyst. *Energy Environ Sci* 2015;8:3563-71. DOI
59. Fan H, Yu H, Zhang Y, et al. Fe-Doped Ni_3C nanodots in N-doped carbon nanosheets for efficient hydrogen-evolution and oxygen-evolution electrocatalysis. *Angew Chem Int Ed Engl* 2017;56:12566-70. DOI PubMed
60. Liu Z, Tan H, Xin J, et al. Metallic intermediate phase inducing morphological transformation in thermal nitridation: Ni_3FeN-based three-dimensional hierarchical electrocatalyst for water splitting. *ACS Appl Mater Interfaces* 2018;10:3699-706. DOI PubMed
61. Deng J, Ren P, Deng D, Yu L, Yang F, Bao X. Highly active and durable non-precious-metal catalysts encapsulated in carbon nanotubes for hydrogen evolution reaction. *Energy Environ Sci* 2014;7:1919-23. DOI
62. Theerthagiri J, Sudha R, Premnath K, Arunachalam P, Madhavan J, Al-mayouf AM. Growth of iron diselenide nanorods on graphene oxide nanosheets as advanced electrocatalyst for hydrogen evolution reaction. *Int J Hydrog Energy* 2017;42:13020-30. DOI
63. Zhang X, Zhu S, Xia L, Si C, Qu F, Qu F. $Ni(OH)_2$-Fe_2P hybrid nanoarray for alkaline hydrogen evolution reaction with superior activity. *Chem Commun (Camb)* 2018;54:1201-4. DOI PubMed
64. Guo X, Feng Z, Lv Z, et al. Formation of uniform FeP hollow microspheres assembled by nanosheets for efficient hydrogen evolution reaction. *Chem Electro Chem* 2017;4:2052-8. DOI
65. Zhu X, Liu M, Liu Y, et al. Carbon-coated hollow mesoporous FeP microcubes: an efficient and stable electrocatalyst for hydrogen evolution. *J Mater Chem A* 2016;4:8974-7. DOI
66. Chung DY, Jun SW, Yoon G, et al. Large-scale synthesis of carbon-shell-coated FeP nanoparticles for robust hydrogen evolution reaction electrocatalyst. *J Am Chem Soc* 2017;139:6669-74. DOI PubMed
67. Konkena B, Junge Puring K, Sinev I, et al. Pentlandite rocks as sustainable and stable efficient electrocatalysts for hydrogen generation. *Nat Commun* 2016;7:12269. DOI PubMed PMC
68. Yu J, Cheng G, Luo W. Ternary nickel-iron sulfide microflowers as a robust electrocatalyst for bifunctional water splitting. *J Mater Chem A* 2017;5:15838-44. DOI
69. Li Y, Wang Y, Pattengale B, et al. High-index faceted $CuFeS_2$ nanosheets with enhanced behavior for boosting hydrogen evolution reaction. *Nanoscale* 2017;9:9230-7. DOI PubMed
70. Man IC, Su H, Calle-vallejo F, et al. Universality in oxygen evolution electrocatalysis on oxide surfaces. *ChemCatChem* 2011;3:1159-65. DOI
71. Rasiyah P, Tseung ACC. A mechanistic study of oxygen evolution on Li-doped Co_3O_4. *J Electrochem Soc* 1983;130:365-8. DOI
72. Wang HY, Hung SF, Chen HY, Chan TS, Chen HM, Liu B. In operando identification of geometrical-site-dependent water oxidation

activity of spinel Co_3O_4. *J Am Chem Soc* 2016;138:36-9. DOI PubMed
73. Menezes PW, Indra A, Gutkin V, Driess M. Boosting electrochemical water oxidation through replacement of O_hCo sites in cobalt oxide spinel with manganese. *Chem Commun* 2017;53:8018-21. DOI PubMed
74. Xu L, Jiang Q, Xiao Z, et al. Plasma-engraved Co_3O_4 nanosheets with oxygen vacancies and high surface area for the oxygen evolution reaction. *Angew Chem Int Ed Engl* 2016;55:5277-81. DOI PubMed
75. Tong Y, Chen P, Zhou T, et al. A bifunctional hybrid electrocatalyst for oxygen reduction and evolution: cobalt oxide nanoparticles strongly coupled to B, N-decorated graphene. *Angew Chem* 2017;129:7227-31. DOI PubMed
76. Bothra P, Pati SK. Activity of water oxidation on pure and (Fe, Ni, and Cu)-substituted Co_3O_4. *ACS Energy Lett* 2016;1:858-62. DOI
77. Lin C, Mccrory CCL. Effect of chromium doping on electrochemical water oxidation activity by $Co_{3-x}Cr_xO_4$ spinel catalysts. *ACS Catal* 2017;7:443-51. DOI
78. Tahir M, Pan L, Zhang R, et al. High-valence-state NiO/Co_3O_4 Nanoparticles on nitrogen-doped carbon for oxygen evolution at low overpotential. *ACS Energy Lett* 2017;2:2177-82. DOI
79. Patel M, Park W, Ray A, Kim J, Lee J. Photoelectrocatalytic sea water splitting using Kirkendall diffusion grown functional Co_3O_4 film. *Sol Energy Mater Sol Cells* 2017;171:267-74. DOI
80. Chen S, Wei Z, Qi X, et al. Nanostructured polyaniline-decorated Pt/C@PANI core-shell catalyst with enhanced durability and activity. *J Am Chem Soc* 2012;134:13252-5. DOI PubMed
81. Feng JX, Ding LX, Ye SH, et al. $Co(OH)_2$ @PANI hybrid nanosheets with 3D networks as high-performance electrocatalysts for hydrogen evolution reaction. *Adv Mater* 2015;27:7051-7. DOI
82. Sun X, Liu X, Liu R, Sun X, Li A, Li W. PANI@Co-FeLDHs as highly efficient electrocatalysts for oxygen evolution reaction. *Catal Commun* 2020;133:105826. DOI
83. Dang W, Shen Y, Lin M, Jiao H, Xu L, Wang Z. Noble-metal-free electrocatalyst based on a mixed CoNi metal-organic framework for oxygen evolution reaction. *J Alloys Compd* 2019;792:69-76. DOI
84. Chen X, Chen Y, Luo X, et al. Polyaniline engineering defect-induced nitrogen doped carbon-supported Co_3O_4 hybrid composite as a high-efficiency electrocatalyst for oxygen evolution reaction. *Appl Surf Sci* 2020;526:146626. DOI
85. Wang C, Li Z, Wang L, Lu X, Wang S, Niu X. Vertical-space-limit synthesis of bifunctional Fe, N-codoped 2D multilayer graphene electrocatalysts for Zn-air battery. *Energy Technol* 2019;7:1900123. DOI
86. Duan Y, Huang Z, Ren J, et al. Highly efficient OER catalyst enabled by in situ generated manganese spinel on polyaniline with strong coordination. *Dalton Trans* 2022;51:9116-26. DOI PubMed
87. Chen X, Chen Y, Shen Z, et al. Self-crosslinkable polyaniline with coordinated stabilized CoOOH nanosheets as a high-efficiency electrocatalyst for oxygen evolution reaction. *Appl Surf Sci* 2020;529:147173. DOI
88. Grosvenor AP, Wik SD, Cavell RG, Mar A. Examination of the bonding in binary transition-metal monophosphides MP (M = Cr, Mn, Fe, Co) by X-ray photoelectron spectroscopy. *Inorg Chem* 2005;44:8988-98. DOI PubMed
89. Ryu J, Jung N, Jang JH, Kim H, Yoo SJ. In situ transformation of hydrogen-evolving CoP nanoparticles: toward efficient oxygen evolution catalysts bearing dispersed morphologies with Co-oxo/hydroxo molecular units. *ACS Catal* 2015;5:4066-74. DOI
90. Chang J, Xiao Y, Xiao M, Ge J, Liu C, Xing W. Surface oxidized cobalt-phosphide nanorods as an advanced oxygen evolution catalyst in alkaline solution. *ACS Catal* 2015;5:6874-8. DOI
91. Xiao X, He C, Zhao S, et al. A general approach to cobalt-based homobimetallic phosphide ultrathin nanosheets for highly efficient oxygen evolution in alkaline media. *Energy Environ Sci* 2017;10:893-9. DOI
92. Mendoza-Garcia A, Zhu H, Yu Y, et al. Controlled anisotropic growth of Co-Fe-P from Co-Fe-O nanoparticles. *Angew Chem Int Ed Engl* 2015;54:9642-5. DOI PubMed
93. Ganesan P, Prabu M, Sanetuntikul J, Shanmugam S. Cobalt sulfide nanoparticles grown on nitrogen and sulfur codoped graphene oxide: an efficient electrocatalyst for oxygen reduction and evolution reactions. *ACS Catal* 2015;5:3625-37. DOI
94. Qiao X, Jin J, Fan H, Li Y, Liao S. In situ growth of cobalt sulfide hollow nanospheres embedded in nitrogen and sulfur co-doped graphene nanoholes as a highly active electrocatalyst for oxygen reduction and evolution. *J Mater Chem A* 2017;5:12354-60. DOI
95. Cai P, Huang J, Chen J, Wen Z. Oxygen-containing amorphous cobalt sulfide porous nanocubes as high-activity electrocatalysts for the oxygen evolution reaction in an alkaline/neutral medium. *Angew Chem Int Ed Engl* 2017;56:4858-61. DOI PubMed
96. Chauhan M, Reddy KP, Gopinath CS, Deka S. Copper cobalt sulfide nanosheets realizing a promising electrocatalytic oxygen evolution reaction. *ACS Catal* 2017;7:5871-9. DOI
97. Sun W, Wei W, Chen N, et al. In situ confined vertical growth of a 1D-$CuCo_2S_4$ nanoarray on Ni foam covered by a 3D-PANI mesh layer to form a self-supporting hierarchical structure for high-efficiency oxygen evolution catalysis. *Nanoscale* 2019;11:12326-36. DOI PubMed
98. Shit SC, Khilari S, Mondal I, Pradhan D, Mondal J. The design of a new cobalt sulfide nanoparticle implanted porous organic polymer nanohybrid as a smart and durable water-splitting photoelectrocatalyst. *Chemistry* 2017;23:14827-38. DOI PubMed
99. Zhou Z, Chen J, Wang Q, Jiang X, Shen Y. Enhanced photoelectrochemical water splitting using a cobalt-sulfide-decorated $BiVO_4$ photoanode. *Chinese J Catal* 2022;43:433-41. DOI
100. Lee DU, Fu J, Park MG, Liu H, Ghorbani Kashkooli A, Chen Z. Self-assembled $NiO/Ni(OH)_2$ nanoflakes as active material for high-power and high-energy hybrid rechargeable battery. *Nano Lett* 2016;16:1794-802. DOI PubMed
101. Tkalych AJ, Zhuang HL, Carter EA. A density functional + U assessment of oxygen evolution reaction mechanisms on β-NiOOH. *ACS Catal* 2017;7:5329-39. DOI

102. Ramakrishnan P, Sohn JI, Sanetuntikul J, Kim JH. In-situ growth of nitrogen-doped mesoporous carbon nanostructure supported nickel metal nanoparticles for oxygen evolution reaction in an alkaline electrolyte. *Electrochim Acta* 2019;306:617-26. DOI
103. Li J, Huang W, Wang M, et al. Low-crystalline bimetallic metal-organic framework electrocatalysts with rich active sites for oxygen evolution. *ACS Energy Lett* 2019;4:285-92. DOI
104. Wang X, Xiao H, Li A, et al. Constructing NiCo/Fe_3O_4 heteroparticles within MOF-74 for efficient oxygen evolution reactions. *J Am Chem Soc* 2018;140:15336-41. DOI PubMed
105. Pan Q, Li S, Tong K, et al. Engineering Ni^{3+} inside nickel selenide as efficient bifunctional oxygen electrocatalysts for Zn-air batteries. *J Mater Sci* 2019;54:9063-74. DOI
106. Swesi AT, Masud J, Nath M. Nickel selenide as a high-efficiency catalyst for oxygen evolution reaction. *Energy Environ Sci* 2016;9:1771-82. DOI
107. Gu C, Hu S, Zheng X, et al. Synthesis of sub-2 nm iron-doped $NiSe_2$ nanowires and their surface-confined oxidation for oxygen evolution catalysis. *Angew Chem Int Ed Engl* 2018;57:4020-4. DOI PubMed
108. Liu PF, Zhang L, Zheng LR, Yang HG. Surface engineering of nickel selenide for an enhanced intrinsic overall water splitting ability. *Mater Chem Front* 2018;2:1725-31. DOI
109. Hou Y, Qiu M, Nam G, et al. Integrated hierarchical cobalt sulfide/nickel selenide hybrid nanosheets as an efficient three-dimensional electrode for electrochemical and photoelectrochemical water splitting. *Nano Lett* 2017;17:4202-9. DOI PubMed
110. Lee S, Cha S, Myung Y, et al. Orthorhombic $NiSe_2$ nanocrystals on Si nanowires for efficient photoelectrochemical water splitting. *ACS Appl Mater Interfaces* 2018;10:33198-204. DOI PubMed
111. Dou Y, Zhang L, Xu J, et al. Dou Y, Zhang L, Xu J, et al. Manipulating the architecture of atomically thin transition metal (hydr)oxides for enhanced oxygen evolution catalysis. *ACS Nano* 2018;12:1878-86. DOI
112. Stamenkovic VR, Strmcnik D, Lopes PP, Markovic NM. Energy and fuels from electrochemical interfaces. *Nat Mater* 2016;16:57-69. DOI PubMed
113. Luan C, Liu G, Liu Y, et al. Structure effects of 2D materials on α-nickel hydroxide for oxygen evolution reaction. *ACS Nano* 2018;12:3875-85. DOI PubMed
114. Gao M, Sheng W, Zhuang Z, et al. Efficient water oxidation using nanostructured α-nickel-hydroxide as an electrocatalyst. *J Am Chem Soc* 2014;136:7077-84. DOI PubMed
115. Li Y, Selloni A. Mechanism and activity of water oxidation on selected surfaces of pure and Fe-doped NiO_x. *ACS Catal* 2014;4:1148-53. DOI
116. Corrigan DA. The catalysis of the oxygen evolution reaction by iron impurities in thin film nickel oxide electrodes. *J Electrochem Soc* 1987;134:377-84. DOI
117. Trotochaud L, Ranney JK, Williams KN, Boettcher SW. Solution-cast metal oxide thin film electrocatalysts for oxygen evolution. *J Am Chem Soc* 2012;134:17253-61. DOI PubMed
118. Fidelsky V, Toroker MC. Enhanced water oxidation catalysis of nickel oxyhydroxide through the addition of vacancies. *J Phys Chem C* 2016;120:25405-10. DOI
119. Friebel D, Louie MW, Bajdich M, et al. Identification of highly active Fe sites in (Ni,Fe)OOH for electrocatalytic water splitting. *J Am Chem Soc* 2015;137:1305-13. DOI PubMed
120. Wu Z, Zou Z, Huang J, Gao F. Fe-doped NiO mesoporous nanosheets array for highly efficient overall water splitting. *J Catal* 2018;358:243-52. DOI
121. Li P, Duan X, Kuang Y, et al. Tuning electronic structure of NiFe layered double hydroxides with vanadium doping toward high efficient electrocatalytic water oxidation. *Adv Energy Mater* 2018;8:1703341. DOI
122. Li L, Xiao S, Li R, et al. Nanotube array-like WO_3 photoanode with dual-layer oxygen-evolution cocatalysts for photoelectrocatalytic overall water splitting. *ACS Appl Energy Mater* 2018;1:6871-80. DOI
123. Wei L, Guo Z, Jia X. Probing photocorrosion mechanism of CdS films and enhancing photoelectrocatalytic activity via cocatalyst. *Catal Lett* 2021;151:56-66. DOI
124. Pirkarami A, Rasouli S, Ghasemi E. 3-D CdS@NiCo layered double hydroxide core-shell photoelectrocatalyst used for efficient overall water splitting. *Appl Catal B* 2019;241:28-40. DOI
125. De S, Zhang J, Luque R, Yan N. Ni-based bimetallic heterogeneous catalysts for energy and environmental applications. *Energy Environ Sci* 2016;9:3314-47. DOI
126. Zhang R, Wang X, Yu S, et al. Ternary $NiCo_2P_x$ nanowires as pH-universal electrocatalysts for highly efficient hydrogen evolution reaction. *Adv Mater* 2017;29:1605502. DOI PubMed
127. Li Y, Jiang Z, Huang J, Zhang X, Chen J. Template-synthesis and electrochemical properties of urchin-like NiCoP electrocatalyst for hydrogen evolution reaction. *Electrochim Acta* 2017;249:301-7. DOI
128. Wang L, Li Y, Xia M, et al. Ni nanoparticles supported on graphene layers: an excellent 3D electrode for hydrogen evolution reaction in alkaline solution. *J Power Sources* 2017;347:220-8. DOI
129. Wang L, Li Y, Yin X, et al. Coral-like-structured Ni/C_3N_4 composite coating: an active electrocatalyst for hydrogen evolution reaction in alkaline solution. *ACS Sustainable Chem Eng* 2017;5:7993-8003. DOI
130. Wang H, Xie Y, Cao H, et al. Flower-like nickel phosphide microballs assembled by nanoplates with exposed high-energy (001) facets: efficient electrocatalyst for the hydrogen evolution reaction. *ChemSusChem* 2017;10:4899-908. DOI PubMed
131. Wang X, Kolen'ko YV, Bao XQ, Kovnir K, Liu L. One-step synthesis of self-supported nickel phosphide nanosheet array cathodes

for efficient electrocatalytic hydrogen generation. *Angew Chem Int Ed Engl* 2015;54:8188-92. DOI PubMed

132. Lado JL, Wang X, Paz E, et al. Design and synthesis of highly active Al-Ni-P foam electrode for hydrogen evolution reaction. *ACS Catal* 2015;5:6503-8. DOI

133. Tong M, Wang L, Yu P, et al. Ni_3S_2 nanosheets in situ epitaxially grown on nanorods as high active and stable homojunction electrocatalyst for hydrogen evolution reaction. *ACS Sustainable Chem Eng* 2018;6:2474-81. DOI

134. Yang CL, Chen JP, Wei KC, Chen JY, Huang CW, Liao ZX. Release of doxorubicin by a folate-grafted, chitosan-coated magnetic nanoparticle. *Nanomaterials* 2017;7:85. DOI PubMed PMC

135. Long X, Li G, Wang Z, et al. Metallic iron-nickel sulfide ultrathin nanosheets as a highly active electrocatalyst for hydrogen evolution reaction in acidic media. *J Am Chem Soc* 2015;137:11900-3. DOI PubMed

136. Qu Y, Yang M, Chai J, et al. Facile synthesis of vanadium-doped Ni_3S_2 nanowire arrays as active electrocatalyst for hydrogen evolution reaction. *ACS Appl Mater Interfaces* 2017;9:5959-67. DOI PubMed

137. Wang P, Zhang X, Zhang J, et al. Precise tuning in platinum-nickel/nickel sulfide interface nanowires for synergistic hydrogen evolution catalysis. *Nat Commun* 2017;8:14580. DOI PubMed PMC

138. Zheng S, Li X, Yan B, et al. Transition-metal (Fe, Co, Ni) based metal-organic frameworks for electrochemical energy storage. *Adv Energy Mater* 2017;7:1602733. DOI